ORNL/TM-2006-547

OAK RIDGE NATIONAL LABORATORY
MANAGED BY UT-BATTELLE FOR THE DEPARTMENT OF ENERGY

Status of Testing and Characterization of CMS Alloy 617 and Alloy 230

Weiju Ren, Terry Totemeier
Mike Santella, Rick Battiste, Denis E. Clark

August 31, 2006

UT-BATTELLE
OAK RIDGE NATIONAL LABORATORY

ORNL/TM-2006-547

Status of Testing and Characterization of CMS Alloy 617 and Alloy 230

Weiju Ren, Mike Santella & Rick Battiste
Materials Science and Technology Division
Oak Ridge National Laboratory

Terry C. Totemeier & Denis E. Clark
Material Sciences
Idaho National Laboratory

August 31, 2006

Prepared for

Office of Nuclear Energy

Prepared by
OAK RIDGE NATIONAL LABORATORY
Oak Ridge, Tennessee 37831
managed by
UT-BATTELLE, LLC
for the
U.S. DEPARTMENT OF ENERGY
Under DOE Contract No. DE-AC05-00OR22725

ABTRACT

Status and progress in testing and characterizing CMS Alloy 617 and Alloy 230 tasks in FY06 at ORNL and INL are described. ORNL research has focused on CMS Alloy 617 development and creep and tensile properties of both alloys. In addition to refurbishing facilities to conduct tests, a significant amount of creep and tensile data on Alloy 230, worth several years of research funds and time, has been located and collected from private enterprise.

INL research has focused on the creep-fatigue behavior of standard chemistry Alloy 617 base metal and fusion weldments. Creep-fatigue tests have been performed in air, vacuum, and purified Ar environments at 800 and 1000°C. Initial characterization and high-temperature joining work has also been performed on Alloy 230 and CCA Alloy 617 in preparation for creep-fatigue testing.

CONTENTS

ACKNOWLEDEMENTS

The ORNL author is grateful to William Corwin for programmatic direction and constructive comments; to Mike Santella and Rick Battiste for significant contributions to CMS Alloy 617 development and mechanical testing facilities refurbishment, respectively; to Ed Hatfield, Tom Geer, Robbie Reed, David Thomas, Scott Bell and Darin DeFalco for technical support.

This work is sponsored by the U.S. Department of Energy, Office of Nuclear Energy Science and Technology under contract DE-AC05-00OR22725 with Oak Ridge National Laboratory, managed by UT-Battelle, LLC.

1. INTRODUCTION

In developing the Gen IV nuclear reactor systems, Alloy 617 and Alloy 230 are considered as primary candidate materials for reactor internals, intermediate heat exchangers, hydrogen heat exchangers, and many other reactor system components [1, 2]. The proposed Gen IV nuclear reactor concepts require some unprecedented working conditions for the structural materials. In the Very High Temperature Reactor (VHTR) concept, the structural alloys must be able to perform at temperatures up to 950ºC (1742ºF) in helium environment for service lives up to 60 years. To qualify the candidate materials for reactor design and construction, sufficient data on mechanical properties must be provided for materials selection, model development, and codification under the American Society of Mechanical Engineers Boiler and Pressure Vessel Codes and Standards.

Alloy 617 and Alloy 230 are both nickel base superalloys developed for high temperature service with a good combination of high-temperature strength and oxidation resistance, as well as excellent resistance to a wide range of corrosive environments. Alloy 617 was introduced into the marketplace in the early 1970s, and a significant amount of mechanical property data, in both air and helium testing environments, has been generated over the past several decades [3]. However, reviews of the collected existing data have revealed that many of the datasets are incomplete, missing important information such as pedigree and original test data curves that are needed for studies and modeling required for the Gen IV nuclear reactor development. Data gaps also exist, especially in the very high temperature range required for VHTR applications. Furthermore, significant data scatter has been observed in mechanical properties [4]. The data scatter would necessitate large safety and knockdown factors, leaving very limited allowable strengths for reactor component design. Compared to Alloy 617, Alloy 230 is a relatively new alloy with the possibility to outperform Alloy 617 in fatigue and thermal fatigue properties desired for the Gen IV reactor working conditions [5 – 7]. However, because it is new, existing data is lacking, especially in helium environment needed for the VHTR.

A comprehensive testing plan was developed in 2004 to provide guidance for high temperature metallic materials data generation [8]. Microstructural characterization was also recommended in the test plan to gain a mechanistic understanding of materials behavior, which is crucial for predicting long-term properties evolution. Analysis of the data scatter in Alloy 617 suggests that the wide chemistry range of the ASTM/ASME standard specifications may be one of the significant contributing factors. In FY05, a task was conducted to evaluate this issue and provide guidance for developing a controlled material specification of Alloy 617 (CMS Alloy 617). The strategy was to refine Alloy 617 within the ASTM/ASME standard specification limits with the main goal of reducing data scatter, and if possible, achieving improved high temperature strength. A report was completed in May 2005 on the evaluation, and some recommendations were made for CMS Alloy 617 development [4].

Data generation tasks are defined for FY06 for both the Idaho National Laboratory (INL) and the Oak Ridge National Laboratory (ORNL). The efforts include developing the CMS Alloy 617 with limited funding ($50K), purchasing CMS Alloy 617 and Alloy 230 for testing, establishing and/or refurbishing testing facilities, designing and preparing testing procedures and specimens, and completing scoping tests for FY07 testing expansion. In April, an INL/ORNL joint report

on procurement and initial characterization of both alloys was completed and submitted to the Department of Energy (DOE) [9]. The present report is a follow-up of the April report, but the focus is shifted to the status of CMS Alloy 617 development and testing and characterization of the two alloys.

2. STATUS OF CMS ALLOY 617 DEVELOPMENT (W. Ren & M. Santella, ORNL)

2.1 Manufacturing Issues in the Development of CMS Alloy 617

Early experimental progress on CMS Alloy 617 was briefly summarized in the April report [9]. For documentation purposes, some details of the development will be described in the present report. The experimental study was conducted mainly to address concerns raised by computer modeling results and suggestions made by three major manufacturers of Alloy 617, including Special Metals, ThyssenKrupp VDM, and Haynes International. Computational thermo modeling conducted at ORNL using ThermoCalc suggested possible formation of undesirable sigma phase at the maximum chemistry of the ASTM/ASME standard specification. Since the CMS Alloy 617 specification was to be developed within the ASTM/ASME standard specification, the sigma phase could also form in CMS Alloy 617. This possibility was supported by computational modeling conducted at Special Metals using the JMat Pro program [10]. For the proposed CMS Alloy 617 chemistry [4], several suggestions were made by the manufacturers at an ORNL workshop held in the first month of FY06. It was pointed out by Special Metals and ThyssenKrupp VDM that the 1.0% Fe concentration originally proposed for the CMS Alloy 617 as shown in Table 1 was too tight for fabrication. They suggested a concentration range of 1.5 ~ 2.0% Fe. Meanwhile, Haynes International indicated that 1.0% Fe could be fabricated but the cost would be increased. ThyssenKrupp VDM also suggested that the concentration ranges of 1.20 ~ 1.40% Al and 0.40 ~ 0.60% Ti were also too tight for fabrication and could very likely increase the cost. Special Metals further suggested that keeping Cr, Co, and Mo at high levels at the same time for improved creep strength could make the material processing difficult. The manufacturers suggested that experimental investigation be conducted on hot workability and cold workability of CMS Alloy 617. Based on those suggestions, a total of seven heats of various adjusted chemistries of Alloy 617 were designed for analysis, and four

Table 1: ASTM/ASEM standard chemical specification for Alloy 617 and the initial tentative chemical specification for CMS Alloy 617 (wt. %)

Heat	**Ni**	**Cr**	**Co**	**Mo**	**Fe**	**Mn**	**Al**	**C**
ASTM Max	-	24.0	15.0	10.0	3.0	1.0	1.5	0.15
ASTM Min	44.5	20.0	10.0	8.0	-	-	0.8	0.05
CMS Max		24.0	15.0	10.0	1.0	1.0	1.40	0.10
CMS Min	44.5	22.0	13.0	9.0	-	-	1.20	0.07
Heat	**Cu**	**Si**	**S**	**Ti**	**P**	**B**	**N**	**Nb**
ASTM Max	0.5	1.0	0.015	0.6	-	0.006	-	-
ASTM Min	-	-	-	-	-	-	-	-
CMS Max	0.2	0.3	0.008	0.60	0.010	0.005	0.040	-
CMS Min	-	-	-	0.40	-	0.002	-	-

10-lb heats from the seven adjusted chemistries were produced for experimental investigation including microstructural characterization and Gleeble hot workability testing.

The computational thmodynamics modeling results of the maximum and minimum chemistries of the ASTM/ASME standard specification are presented in Fig. 1 and Fig. 2, respectively. Fig. 1 suggests that undesirable sigma phase could form at the maximum chemistry. Usually the sigma phase preferentially forms along the grain boundaries. If it forms

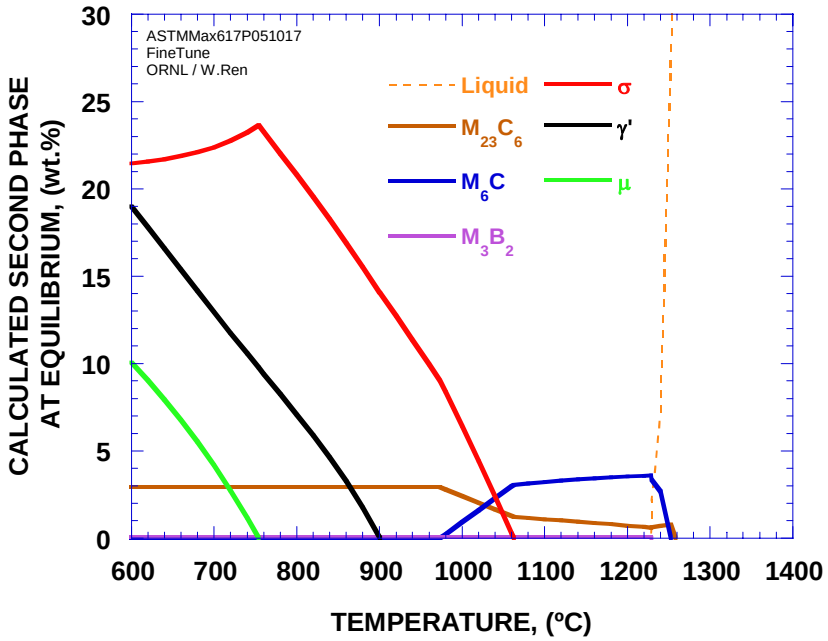

Fig. 1: ThermoCalc modeling result of second phases at various temperatures in equilibrium at the maximum ASTM/ASME specification composition of standard 617

in reactor components, it can cause a detrimental decrease of toughness at lower temperatures occurring during shut-down or heating-up periods. Further modeling calculations also indicated that the major elements for sigma phase formation were Cr, Co, Mo, and Ni, and their concentrations in the sigma phase would vary with temperature. The ThermoCalc modeling calculation was conducted based on an experimental database, and the predictions are usually worth serious consideration.

Since the CMS Alloy 617 development is confined within the ASTM/ASME standard chemistry specification, the possibility of sigma phase formation therefore also exists, and should be avoided through adequately adjusting the chemistry while keeping the strengthening element contents as high as possible. To provide guidance for the adjustment, equilibrium phase diagrams as shown in Fig. 3 were produced through computational modeling. The chemical composition used for producing Fig. 3 was typical of the intended CMS Alloy 617 chemistries including 15.0Co, 8.0Mo, 1.40Al, 0.60Ti, 0.10C, and 0.04N (all in weight percent) with various Cr concentrations. It is apparent from Fig. 3 that for the prescribed composition, the sigma phase

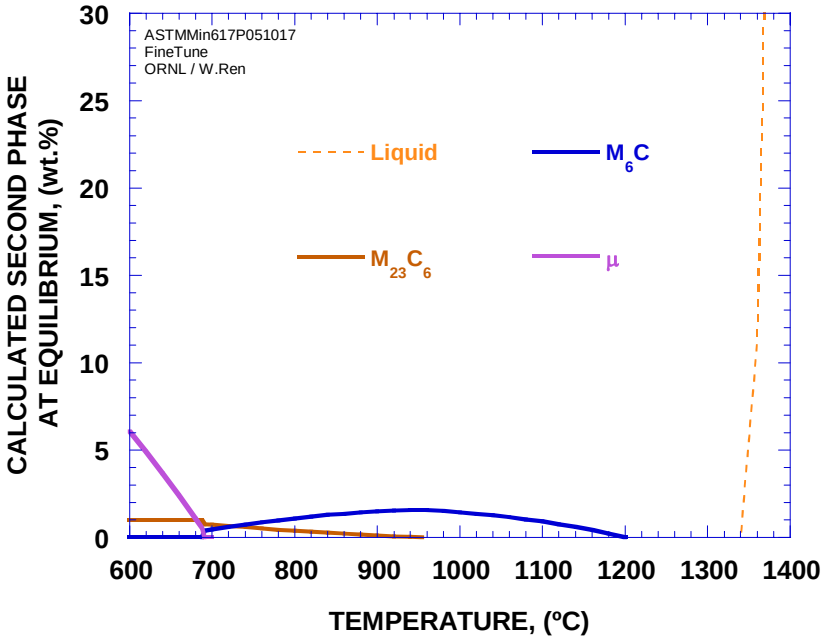

Fig. 2: ThermoCalc modeling result of second phases at various temperatures in equilibrium at the minimum ASTM/ASME specification composition of standard 617

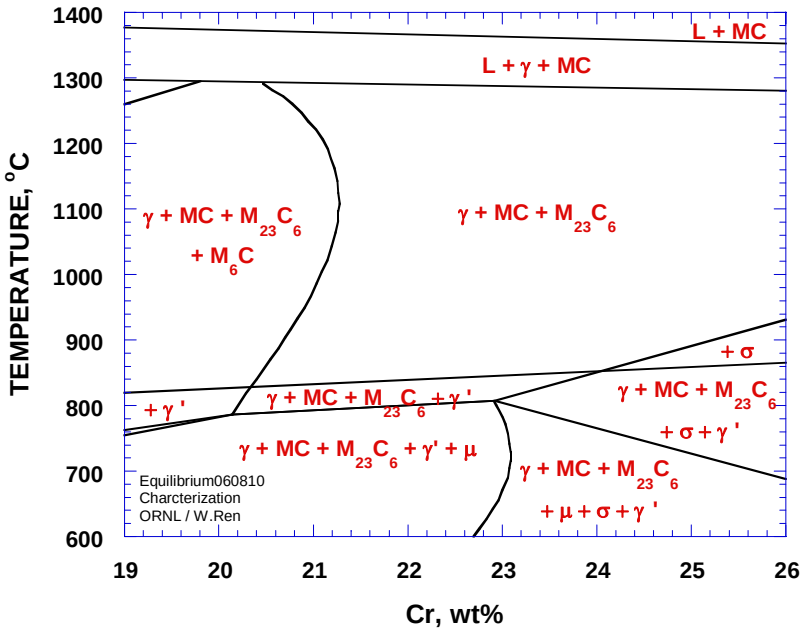

Fig. 3: Calculated equilibrium phase diagram for intended CMS Alloy 617 chemistry combinations

does not appear at 600ºC (1112ºF) and above if Cr is less than 22.7%. Guided by such equilibrium phase diagrams and a maximizing strength principle, various chemistry combinations were calculated. Those with minimized sigma formation were selected for further analysis, and four were eventually manufactured as 10-lb heats for testing and microstructural characterization. Table 2 summaries the selected chemistries with the least sigma formation possibility as well as other considerations that will be discussed later.

Table 2: Summary of the experimental CMS Alloy 617 heat compositions (wt. %)

Heat	Ni	Cr	Co	Mo	Fe	Mn	Al	C
GenIV-1	Bal.	22.0	15.0	8.0	2.0	1.0	1.3	0.09
GenIV-1PA	50.66	21.71	14.80	7.91	2.05	0.97	1.21	0.12
GenIV-2	Bal.	20.0	15.0	10.0	2.0	1.0	1.3	0.09
GenIV-3	Bal.	22.0	15.0	10.0	2.0	1.0	1.3	0.09
GenIV-4	Bal.	24.0	15.0	10.0	2.0	1.0	1.3	0.09
GenIV-5	Bal.	22	15	8	2.0	1.0	1.3	0.09
GenIV-5PA	Bal.	21.66	14.92	8.03	2.03	0.96	1.32	0.107
GenIV-6	Bal.	22	12.5	8.9	0.4	0.0	1.06	0.07
GenIV-6PA	Bal.	21.68	12.54	8.88	0.43	<0.01	1.15	0.07
GenIV-7	Bal.	22	15	10	2.0	1.0	1.30	0.09
GenIV-7PA	Bal.	21.65	14.97	9.95	2.03	0.94	1.35	0.09
Heat	**Cu**	**Si**	**S**	**Ti**	**P**	**B**	**N**	**Mg**
GenIV-1	0.1	0.2	0.004	0.5	0.005	0.004	0.02	-
GenIV-1PA	<0.01	<0.01	0.011	0.66	0.004	0.005	0.075	-
GenIV-2	0.1	0.2	0.004	0.5	0.005	0.004	0.02	-
GenIV-3	0.1	0.2	0.004	0.5	0.005	0.004	0.02	-
GenIV-4	0.1	0.2	0.004	0.5	0.005	0.004	0.02	-
GenIV-5	0.1	0.2	<0.001	0.50	0.003	0.004	0.020	0.035
GenIV-5PA	<0.01	0.01	0.005	0.62	<0.002	0.0047	0.028	<0.01
GenIV-6	0.08	0.1	<0.004	0.36	0.003	0.003	0.016	0.035
GenIV-6PA	<0.01	0.01	0.004	0.49	<0.002	0.0004	0.030	0.01
GenIV-7	0.1	0.2	<0.001	0.50	0.003	0.004	0.020	0.035
GenIV-7PA	<0.01	0.01	0.004	0.63	<0.002	0.0043	0.039	0.01

PA = product analysis

2.2 Experimental Investigation on Sigma Phase Formation

The first 10-lb heat, designated as GenIV-1, was produced as shown in Fig. 4. The heat was made mainly to develop the manufacturing procedures, verify the minimization of sigma phase,

and study compositional effects on workability. The heat was induction melted under argon cover and poured into a graphite permanent mold that was coated with boron nitride powder. After cooling to room temperature, the top surface was cut off to remove possible macrosegregation, and the ingot was grit blasted to remove surface debris. The ingot size was 25.4 mm x 111 mm x 136.5 mm (1" x 4-3/8" x 5-3/8"). A thin slice was first machined vertically from the side of the ingot as shown in Fig. 4 and reserved for future metallurgical

Fig. 4: The GenIV-1 10-lb heat casting

characterization. The second thin slice was used for chemical analysis to determine whether the casting procedures employed had achieved the aim value of each element. The vertical cutting direction would allow chemical analyses on top, middle and bottom of the ingot to identify macrosegregation had it existed. The chemical analysis results are presented in Table 3. It appears in Table 3 that the casting was successful at its first try. There is no macrosegregation from top to bottom, and all the major aim values were achieved within small allowances.

After the chemistry verification, a 25.4 mm x 31.8 mm x 111 mm plate (1" x 1-1/4" x 4-3/8") was machined off from the ingot for Gleeble hot ductility specimen preparation. A total of 12 round bar specimens as shown in Fig. 5 were prepared. The Gleeble specimens were chosen to be prepared in the as-cast condition to investigate the worst hot ductility situation in the small heat size. The rest of the ingot was then annealed at 1200ºC (1832ºF) for 4 hours, and cut into two equal halves. One half was kept as a backup piece. The other was hot rolled at 1000 ~ 1200ºC (1832 ~ 2192ºF) from 25.4 mm to 12.7 mm (1" to ½") through seven reduction passes with reheats in between to maintain the prescribed processing temperature range. After the plate was reduced to 12.7 mm (½"), it was given a visual evaluation of the hot workability, followed by a final annealing at 1149ºC (2100ºF) for 1 hour, and then reserved for cold workability testing if the Gleeble hot ductility testing indicated good results. As shown in Fig. 6, visual observation

of the hot rolled plate indicated acceptable hot workability, which gave approval for proceeding with the Gleeble hot ductility testing. Meanwhile, both the as-cast and annealed plates were sampled for microstructural analysis to examine the extent of sigma phase formation.

Table 3: Chemical analysis results of the experimental CMS Alloy 617 heat GenIV-1 (wt. %)

Heat	Ni	Cr	Co	Mo	Fe	Mn	Al	C
GenIV-1	Bal.	22.0	15.0	8.0	2.0	1.0	1.3	0.09
Top	50.71	21.69	14.80	7.90	2.06	0.97	1.22	0.12
Center	50.62	21.73	14.80	7.92	2.05	0.97	1.21	0.12
Bottom	50.65	21.72	14.81	7.90	2.05	0.97	1.21	0.12
Average	50.66	21.71	14.80	7.91	2.05	0.97	1.21	0.12
Heat	**Cu**	**Si**	**S**	**Ti**	**P**	**B**	**N**	
GenIV-1	0.1	0.2	0.004	0.5	0.005	0.004	0.02	
Top	<0.01	<0.01	0.011	0.62	0.004	0.005	0.071	
Center	<0.01	<0.01	0.012	0.68	0.004	0.005	0.076	
Bottom	<0.01	<0.01	0.011	0.67	0.004	0.005	0.079	
Average	<0.01	<0.01	0.011	0.66	0.004	0.005	0.075	

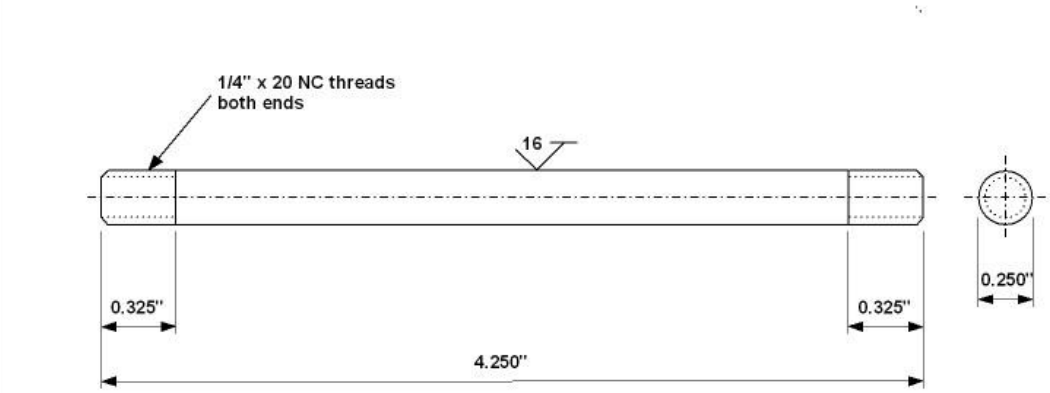

Fig. 5: Gleeble specimen for hot workability investigation

The microstructure of the as-cast GenIV-1 heat is shown in Fig. 7 and Fig. 8. Chemical microsegregation is clearly evident at low magnification. Also, a small number of relatively large angular particles are uniformly distributed throughout the microstructure. Pockets of smaller second-phase particles were also distributed throughout the solidification structure as shown in Fig. 8. To gain some insight into the possible identification of phases in the cast structure the average analyzed composition of GenIV-1 was used to perform a Scheil simulation. The Scheil simulation predicts the solidification temperature range and phases that are likely to form during the solidification process. Prediction of the variations of second phase amounts

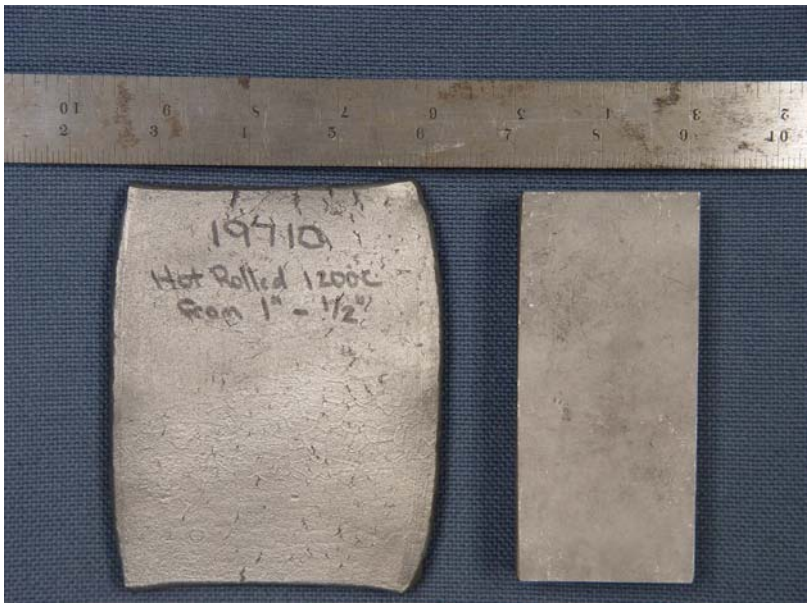

Fig. 6: As-cast and hot rolled halves of the GenIV-1 heat ingot

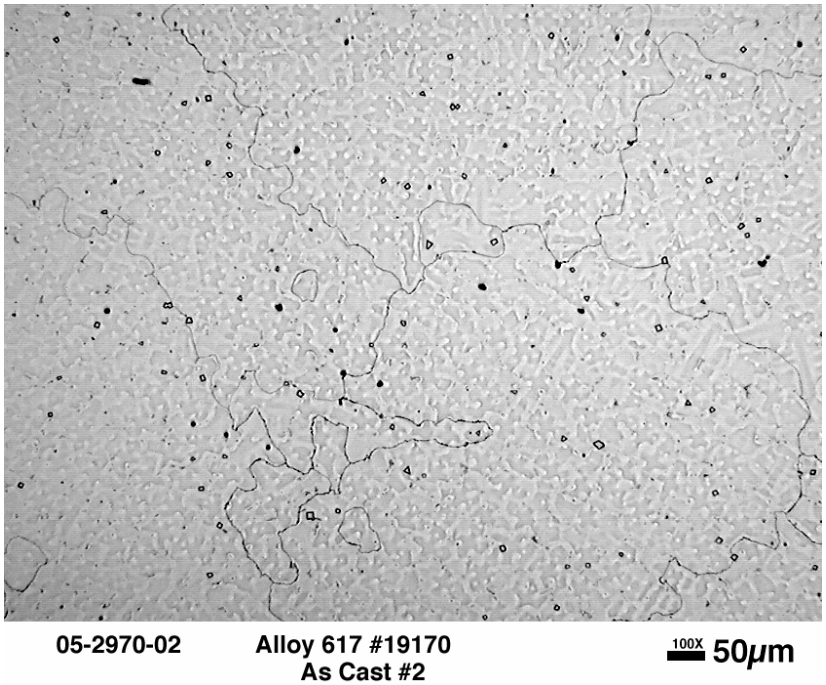

Fig. 7: As-cast microstructure of the GenIV-1 heat ingot at low magnification

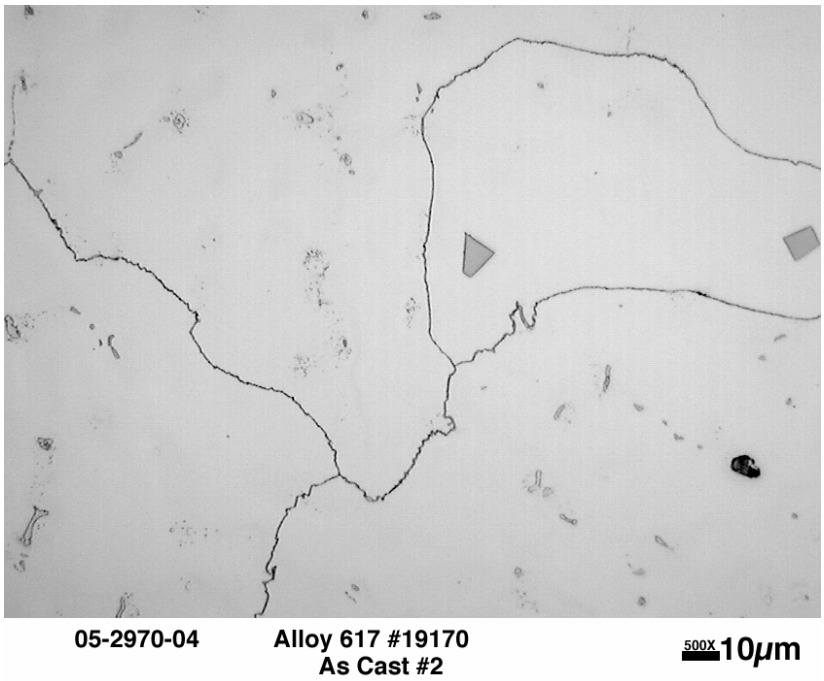

Fig. 8: As-cast microstructure of the GenIV-1 heat ingot at high magnification

with temperature during the solidification processes are plotted in Fig. 9. The solid solution γ phase is not shown in Fig. 9 to more clearly highlight the formation of the second phases. The predicted solidification temperature range for the GenIV-1 composition is 1362 - 1226°C (2484 – 2239ºF). The phases likely to form by the end of solidification are MN, MC, M_6C, $M_{23}C_6$, and sigma phase. As shown in Fig. 9, the MN phase is thermodynamically stable, i. e., it already exists, in the liquid at the time solidification begins at 1362°C (2484ºF). The predicted composition of the MN phase is nearly stoichiometric TiN. The morphology of the large angular particles in Fig. 8 is consistent with this identification. The Scheil simulation indicates that the remaining phases form as solidification proceeds. The predicted compositions and amounts of the phases are given in Table 4. The Scheil results are only representative of the microstructure at the time solidification ends so it does not account for any phase transformations, precipitation, or particle dissolution that may occur during subsequent cooling. However, the results of the simulation for phase amounts appear to agree reasonably well with the observed as-cast microstructure.

The microstructure of the GenIV-1 heat after annealing at 1200ºC (2192ºF) for 4 hours is presented in Figs. 10 and 11. Compared with the microstructure at the same magnification in Fig. 7, the annealed microstructure in Fig. 10 indicates that the intensity of chemical microsegregation is diminished or significantly minimized; at least it is not revealed by etching. Both figures show that the TiN particles are still visible and their size and number appear unchanged from the as-cast condition. Pockets of relatively coarse precipitates are distributed

throughout the microstructure. These precipitates are expected to be coarser $M_{23}C_6$ carbides than found in the as-cast condition. There are also a very small number of small needle-like particles that may be either sigma or carbides. If some of these are sigma, they may be stabilized by the remnant chemical microsegregation. Fig. 11 clearly indicates that grain boundaries are decorated with particles, likely carbides.

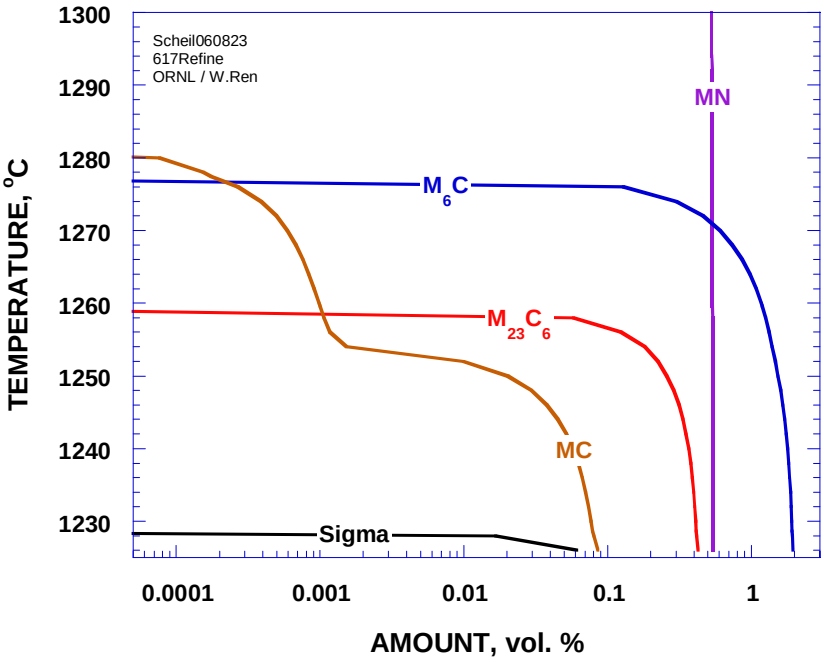

Fig. 9: Results from Scheil simulation for GenIV-1 composition that show second phase formation during solidification

Table 4: Predicted phase amounts and compositions from Scheil simulation of GenIV-1 composition

Phase	Amount (vol %)	Composition
MN	0.54	TiN
MC	0.09	TiC
M_6C	1.95	$(Mo_{.40}Ni_{.31}Cr_{.26}Co_{.03})_6C$
$M_{23}C_6$	0.43	$(Cr_{.67}Ni_{.15}Mo_{.12}Co_{.06})_{23}C_6$
Sigma	0.06	$Cr_{.44}Ni_{.21}Mo_{.18}Co_{.16}Fe_{.02}$

A more detailed microstructural characterization to further investigate the structure and composition of the particles was not performed. However, it is apparent from the above observation that there is no indication of widespread sigma formation. If there is sigma, it appears to be only a small amount that could be dissolved through continued high temperature processing in large commercial size heats.

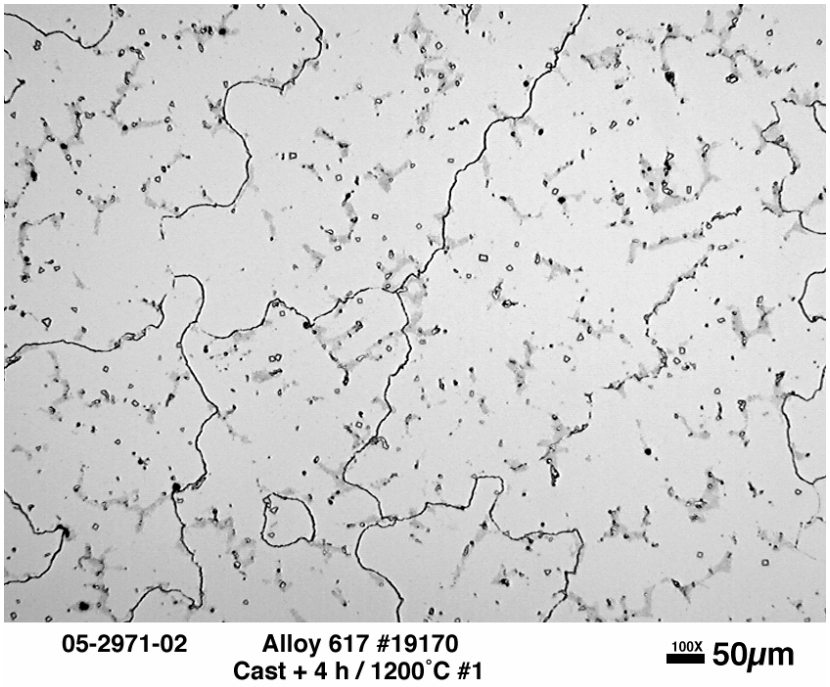

Fig. 10: Annealed microstructure of the GenIV-1 heat ingot at low magnification

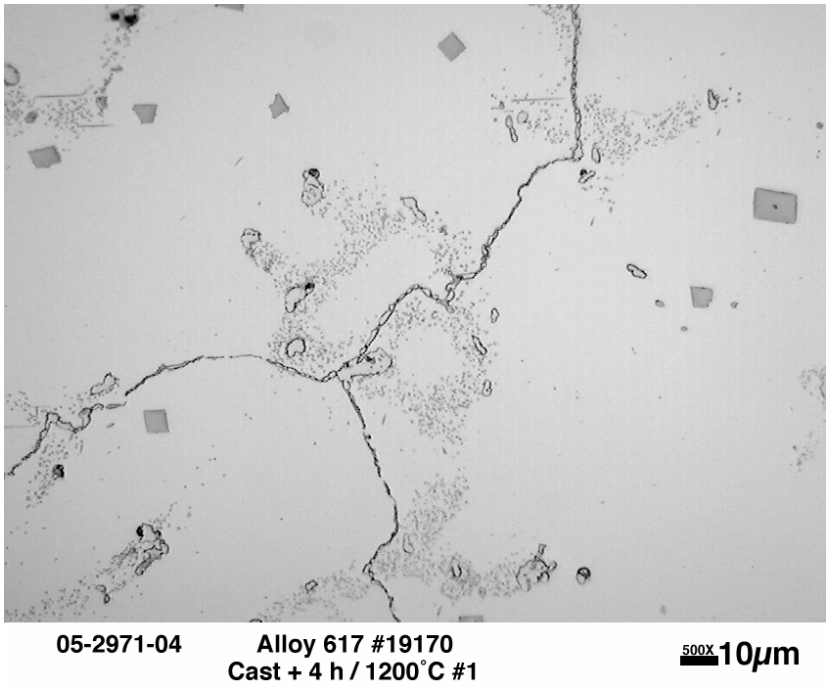

Fig. 11: Annealed microstructure of the GenIV-1 heat ingot at high magnification

2.3 Experimental Investigation on Hot Ductility and Test Results Analysis

The hot ductility tests on the GenIV-1 heat were conducted on Gleeble machine at temperatures ranging from 870 to 1260ºC (1778 to 2322ºF) at a nominal strain rate of 1/s. The test results are compared with a set of commercial heat hot ductility data provided by Special Metals in Fig. 12. It is obvious that the hot ductility of the GenIV-1 heat is much lower than that of the commercial heat. Analysis indicates that many factors could have caused the low hot ductility values in the GenIV-1 heat. The major factors could include:

1. The concentration of sulfur was too high in the GenIV-1 heat;
2. The commercial heat was large in size while the GenIV-1 heat was very small;
3. The commercial heat was heat-treated and hot rolled while the GenIV-1 heat was as-cast;
4. Possible differences in detailed testing procedures and methods for the two heats;
5. Difference in chemical compositions of the two heats.

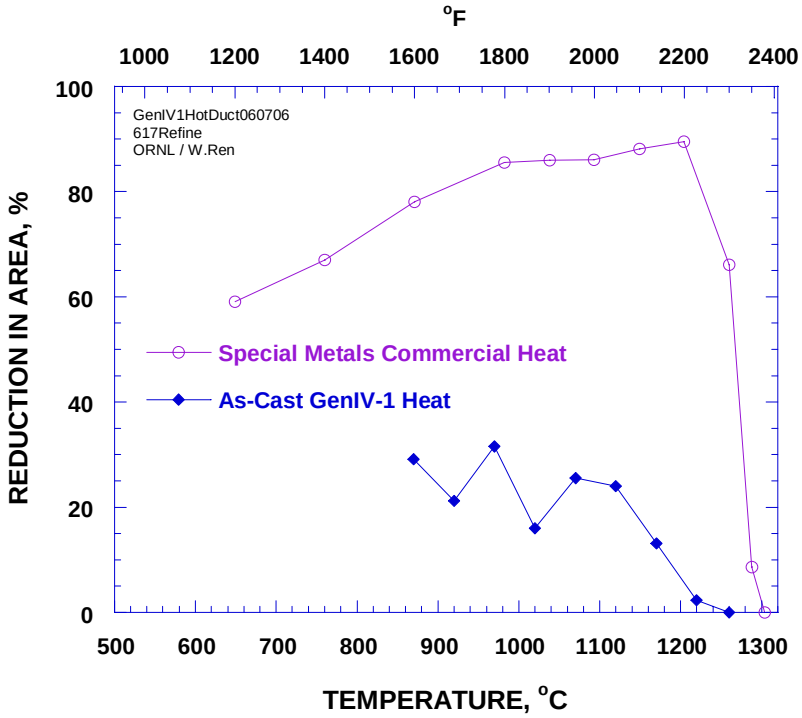

Fig. 12: Comparison of hot ductility between a commercial heat and the as-cast GenIV-1 heat

To investigate the effects of these factors, more 10-lb heats were produced. To address factor 1, the GenIV-5 heat was designed based essentially on the GenIV-1 composition with the addition of magnesium to help controlling the sulfur level below 0.001%. Its phosphorous concentration was also decreased to 0.002% for further assurance of good hot ductility. A product check as shown in Table 2 indicated that both the sulfur and phosphorous concentrations were reduced compared to the actual values in the GenIV-1 heat (the GenIV-5PA values vs. the GenIV-1PA values), but the sulfur content was still higher than the aim value. To accelerate the entire experimental process, the GenIV-7 heat was designed from essentially the GenIV-5

composition with additional 2% Mo for improved creep strength, and the heat was tested first with the GenIV-5 heat as a fallback substitute. A product check indicated that the sulfur concentration of the GenIV-7 heat also did not reach the aim value. A corrective heat was not made in order to keep rapid progress within the available time and budget, especially when the already produced GenIV-7 heat was still considered acceptable for tentative testing to evaluate hot ductility. To address factor 2, the GenIV-6 heat was produced with the average composition of 13 commercial heats that had magnesium for sulfur control. Test of the GenIV-6 heat could provide a baseline for comparison between small size heats. To address factor 3, all three heats would be heat treated and hot rolled before hot ductility testing in compliance with the procedures suggested by Special Metals, which included homogenization of the cast ingot at 1300°C (2372ºF) for 12 hours followed by hot rolling at 1000 ~ 1100ºC (1832 ~ 2012ºF) with inter pass reheats to maintain the hot rolling temperature range. To address factor 4, a plate of commercial heat XX2834UK was machined for comparative hot ductility testing. With the first four factors investigated, factor 5 would become relatively isolated for analysis.

Hot ductility test results of the GenIV-6, GenIV-7 and XX2834UK heats are plotted with those of the previous two heats in Fig. 13. Compared with the GenIV-1 curve, the curve for GenIV-7 obviously exhibits improved hot ductility. The improvement can be attributed to the control of sulfur and phosphorous levels, plus heat treatment and hot rolling. Additional effects from composition on the improvement can be reasonably excluded because beside the controlled sulfur and phosphorous with magnesium, the GenIV-7 composition had additional 2% Mo which tends to decrease hot ductility. Then the question is whether the hot ductility of the GenIV-7 heat is comparable to that of the standard commercial heats.

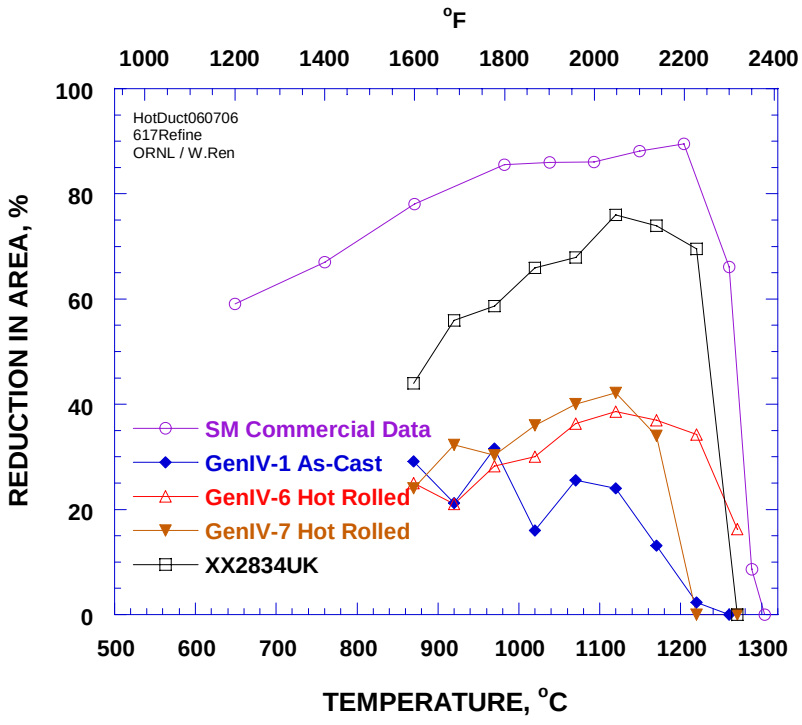

Fig. 13: Comparison of hot ductility among five heats

It can be observed in Fig. 13 that the curves for GenIV-6 and GenIV-7 are comparable, with the GenIV-7 curve slightly higher before temperature reaches approximately 1150ºC (2102ºF). Since the GenIV-6 heat had the average composition of 13 commercial heats, this observation suggests that the GenIV-7 heat had similar hot ductility to commercial composition heats in the same ingot size. Then, what needs to be investigated is whether the GenIV-7 composition could result in high hot ductility comparable to that of standard commercial heats for temperatures up to 1150ºC (2102ºF) if it had the commercial size and processing.

The comparison between the curves of the GenIV-6 and XX2834UK heats in Fig 13 indicates that the XX2834UK heat exhibited much better hot ductility. Beside possible composition effects, the better hot ductility in heat XX2834UK can be reasonably attributed to its large commercial size and significant hot working during its processing. The GenIV-6 and XX2834UK specimens were machined from 12.7 mm (0.5") and 25.4 mm (1") thick plates, respectively. As a common practice, commercial plates are normally reduced to their final thicknesses from the ingot thickness range of 305 ~ 508 mm (12 ~ 20"), with many reheats and annealing between the passes. In contrast, the total reduction of the experimental GenIV-6 heat was only from 25.4 mm (1") to 12.7 mm (0.5"), although it did have multiple passes with reheats in between. With significant thermal processing on the XX2834UK heat, its microstructure is expected to exhibit much improved hot ductility. If the GenIV-6 heat had the commercial size, it could likely demonstrate similar hot ductility as the XX2834UK heat. Based on the discussion on the GenIV-6 and GenIV-7 heats in the last paragraph, the similar improved hot ductility should also be expected in the GenIV-7 heat if it had the commercial ingot size. Of course, it should be reminded that possible composition effects are still excluded in reaching this expectation.

Now the question remains whether possible differences in detailed testing procedures and methods contributed to low hot ductility. The answer may be found in the XX2834UK and SM Commercial Data curves. Both are commercial heats produced by Special Metals. The only known difference is that they were tested at different facilities by different organizations. To this point of the analysis, however, answering this question is no longer important, because it is clear that the XX2834UK heat is a commercial heat with acceptable hot ductility, and its hot ductility curve was generated at ORNL using the same procedures and facilities as the curves of all the GenIV heats. Therefore, the XX2834UK curve can be used as a baseline for comparison.

In the analysis above, one important factor has not been addressed, i. e., the possible compositional effects on hot ductility. Within FY06, it is impossible to thoroughly investigate this factor. However, some reasonable assumptions can be made to assist discussion and analysis. In comparing the GenIV-6 and the XX2834UK heats, it was discussed that if in commercial size, the GenIV-6 heat could likely demonstrate hot ductility similar to that of the XX2834UK heat. The only uncertainty is the possible effects resulting from their compositional difference. This uncertainty, however, can be reasonably excluded based on the fact that Special Metals normally produces its commercial heats in a "comfortable" chemistry range within the ASTM/ASME standard chemistry specification. Furthermore, the hot ductility of a given commercial product form (25.4 mm thick plate in this case) must meet certain standard. Therefore, assumptions can be reasonably made that the hot ductility of the XX2834UK and the

SM Commercial Data heat should actually be comparable if tested in exactly the same conditions. Further, the compositions of the GenIV-6 heat, the XX2834UK, and the SM Commercial Data heat should all fall into the "comfortable" zone with limited differences. The compositional difference effect on hot ductility is therefore little and assumingly negligible.

Based on the above assumptions, the curve for the GenIV-6 heat should be moved up to the level of the XX2834UK curve if the heat had the commercial ingot size; and the curve for the GenIV-7 heat should also be moved up with the GenIV-6 curve if the heat had the commercial ingot size. Then the curves in Fig. 13 should look as shown in Fig. 14, which suggests that the GenIV-7 composition could result in hot ductility that matches the commercial level at temperatures up to approximately 1170ºC (2138ºF). With a better control to restrict sulfur concentration below 0.001%, its hot ductility could be further improved.

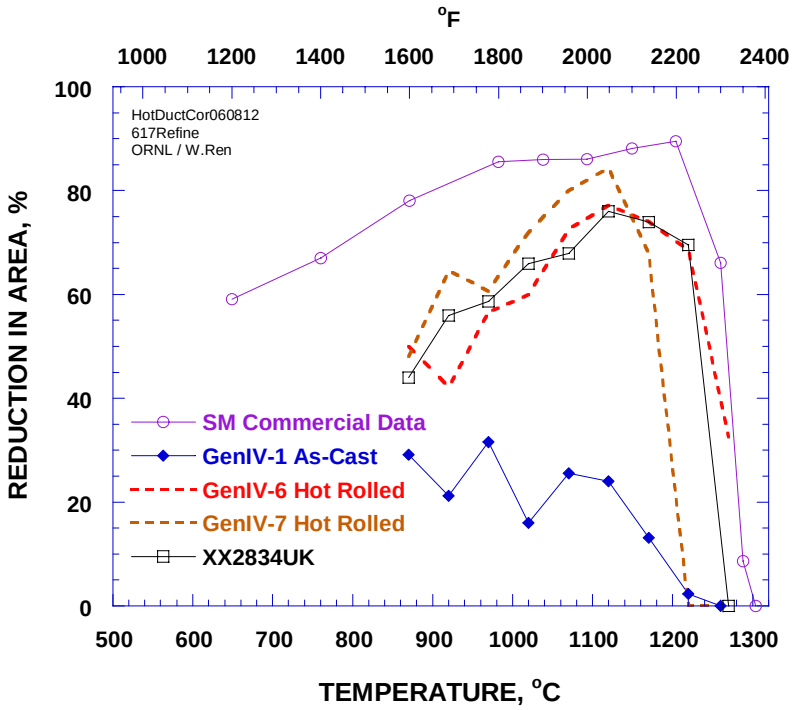

Fig. 14: Comparison of hot ductility with the assumption of no initial ingot size effects on the GenIV-6 and GenIV-7 heats

To finalize the chemistry specification for CMS Alloy 617, more investigations are still needed. Further experimental verifications on the assumptions made in the analysis above are necessary; no matter how reasonable those assumptions may sound.

It is important to point out that both Fig. 13 and Fig. 14 have shown a dramatic hot ductility plummet to zero in the GenIV-7 heat curve at temperatures above 1200ºC (2192ºF). Because the temperature range around 1200ºC (2192ºF) is usually used for hot processing depending on manufacturing procedures and product forms, the sudden drop suggests a potential hot working problem of the GenIV-7 heat in that temperature range. Furthermore, if this problem does exist,

the preliminary results from the GenIV-7 heat suggest that a commercial order to the ASTM/ASME specification, if it happens to fall in the GenIV-7 chemical composition sub-zone, may also have poor workability at temperatures above 1200ºC (2192ºF). There are two options for addressing this issue: we can either restrict the thermal processing temperatures below 1100ºC (2012ºF) whenever possible, or further investigate and eliminate the causes for the problem if time and funding permit.

Preliminary microstructural characterization results of the tested hot ductility specimens from the GenIV-6 and GenIV-7 heats are presented in Fig. 15 and Fig. 16, respectively. Both specimens were tested at 1270ºC (2318ºF) at the strain rate of 1/s. The microstructures in both specimens exhibit intergranular fracture. The GenIV-6 specimen resulted in a RA value of 16%. Some torn texture can be observed in Fig. 15 along the fractured grain boundaries, an indication of ductility. The GenIV-7 specimen yielded a RA value of 0%. It is apparent in Fig. 16 that some grain boundaries are sharply separated. It is possible that some low-melting phases existed on the separated grain boundaries at the testing temperature when the testing tensile load was rapidly applied. More studies are needed to verify this speculation.

Further investigations, if any, should mainly be focused on finalizing the chemistry upper limit by maximizing the strengthening element levels while keeping acceptable hot and cold workability, and finalizing the chemistry lower limit by narrowing the chemistry range while keeping processing economically and technically viable.

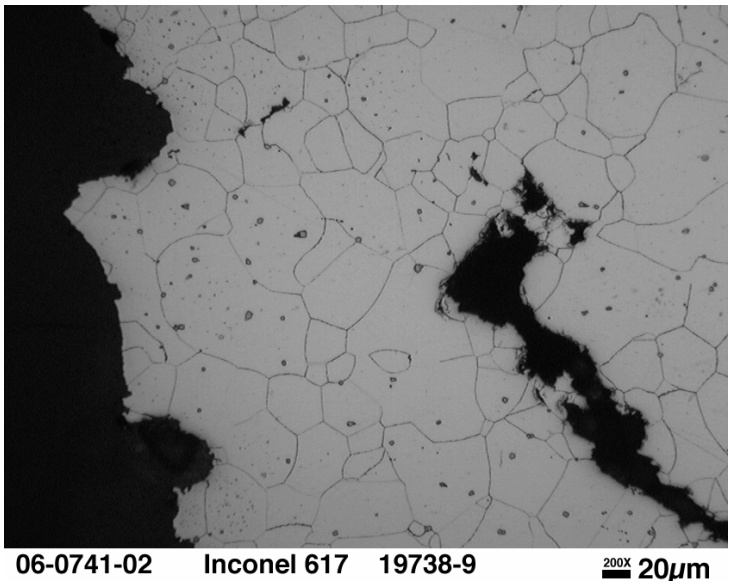

Fig. 15: Fracture of the tested hot ductility specimen from the GenIV-6 heat

It should be stressed that alloy specification development is a time- and funding-demanding process. Experience indicates that it took approximately five years with sufficient funding and manpower for the Modified 9Cr-1Mo steel (Grade 91) to be developed from the standard 9Cr-1Mo steel. Although the experimental cycles in developing CMS Alloy 167 has been extremely

fast on the normal alloy development time scale since its initiation in October of 2005, by January of 2006 it seemed unlikely that satisfactory results could possibly be achieved for placing order to purchase a commercial size heat within the deadline to meet the deliverable requirement of FY 2006. As pointed out in the last paragraph of Section 5.2, "Future Work," in the FY 2005 ORNL report "Development of A Controlled Material Specification for Alloy 617 for Nuclear Applications" [4], when possible lengthy iterations of metallurgical experiments to investigate the effects of the variations in Al, Ti, C, Mo, Co, B, and N on properties of the alloy are needed, a managerial decision must be made based on the required timeframe and funding availability at a certain time of the development. Based on the situation in January, a suggestion was made by INL that while the efforts in experimental small heats was underway, procurement and initial characterization of CMS 617 should have an alternate plan. It was suggested that an existing chemistry controlled variant of Alloy 617, designated as CCA Alloy 617, be acquired and characterized for Gen IV reactor working conditions. It was considered that this alternate plan would not only enable meeting the FY 2006 deliverable requirement, but also provide more choices in the material selection process. At present, the CCA Alloy 617 is temporarily defined as CMS Alloy 617. Final decision needs to be made when preliminary characterization of the alloy is completed and results are analyzed.

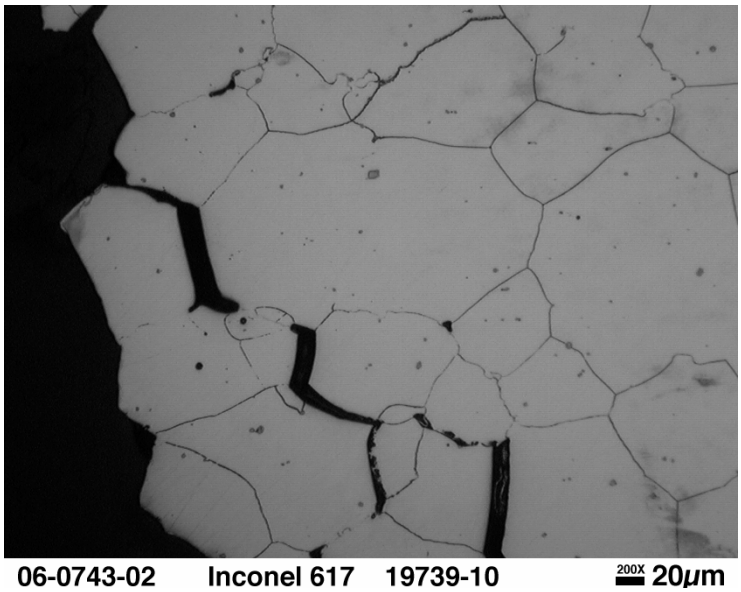

Fig. 16: Fracture of the tested hot ductility specimen from the GenIV-6 heat

3. STATUS OF TESTING AND CHARACTERIZATION (W. Ren & R. Battiste, ORNL)

3.1 Materials

As stipulated in "High Temperature Metallic Materials Test Plan for Generation IV Nuclear Reactors", testing and characterization of the candidate materials should be focused on filling

gaps of existing data to save program funds and time [8]. The CCA Alloy 617 was developed by ThyssenKrupp VDM for the Ultra Supercritical Steam Boiler Project (USC Project) with a target steam working temperature of 760°C (1400ºF). Its composition is presented in Table 5. Only one heat has been produced for this composition. The material has been under investigation for the intended application conditions of the USC Project at ORNL. Preliminary results from the investigation indicated improved creep strength around the intended USC working temperature range, but showed a trend of merging back into the standard strength at higher temperatures. More testing in the higher temperature range must be conducted for verification and data gap filling for the Gen IV reactor working conditions. After negotiation, initial agreement was reached with the USC Project for data and material trading and sharing. The negotiation letter is included in the Appendix for documentation.

Based on the initial agreement, a plate of 50.8 x 304.8 x 990.6 mm (2" x 12" x 39") CCA Alloy 617 was delivered to ORNL from Alstom Power, and a list of tests conducted under the USC Project was also provided to the Gen IV Program. The list included creep testing conditions without the actual test result data. Under the initial agreement, the plate is provided to the Gen IV Program free of charge; in return, the Gen IV Program shall provide a copy of the data generated from the plate to the USC Project. It is planned by the Gen IV Program that in addition to generating data in the high temperature range, some data gaps in the low temperature range will also be filled. Then efforts will be made to further negotiate for trading the low temperature data generated under the USC Project.

Table 5: Chemical composition of the CCA Alloy 617 heat (wt. %)

Heat	**Ni**	**Cr**	**Co**	**Mo**	**Fe**	**Mn**	**Al**	**C**
CCA 617Max	-	23.0	13.0	10.0	1.5	0.3	1.3	0.08
CCA 617Min	Bal.	21.0	11.0	8.0	-	-	0.8	0.05
CCA 617PA[a]	Bal.	21.5	11.3	8.6	0.7	0.03	1.24	0.06
Heat	**Cu**	**Si**	**S**	**Ti**	**P**	**B**	**N**	**Nb**
CCA 617Max	0.05	0.3	0.008	0.5	0.012	0.005	0.050	-
CCA 617Min	-	-	-	0.3	-	0.002	-	-
CCA 617PA[a]	0.01	0.1	<0.001	0.39	0.003	0.003	0.013	0.02

a) Product analysis

Alloy 230 was received as plates cut from Heat 8305 5 7896 procured by INL from Haynes International. The plates conform to American Society of Testing and Materials (ASTM) specification B 435 and American Society of Mechanical Engineers (ASME) specification SB 435. Each plate is 19 mm x 254 mm x 381 mm (0.75" x 10" x 15") in dimension. The grain sized certified by the vendor is ASTM 4.5. Chemical composition of the plates certified by the vendor is given in Table 6.

Table 6: Chemical composition of Alloy 230 plate (wt.%), Haynes heat number 8305 5 7896

Ni	**Cr**	**W**	**Fe**	**Mo**	**Co**	**Mn**	**Si**	**C**	**Al**	**Ti**	**Cu**	**P**	**S**	**B**
Bal	22.43	13.91	1.34	1.34	0.21	0.53	0.37	0.11	0.29	<0.01	0.04	0.005	<0.002	0.004

3.2 Specimen Preparation

The CCA Alloy 617 plate received from Alstom Power was cut into 6 smaller pieces as shown in Fig. 17. The piece designated as Plate C was shipped for testing at INL. Plates B, D, E1, and E2 were machined into specimens for testing at ORNL. Plate A was reserved for future use.

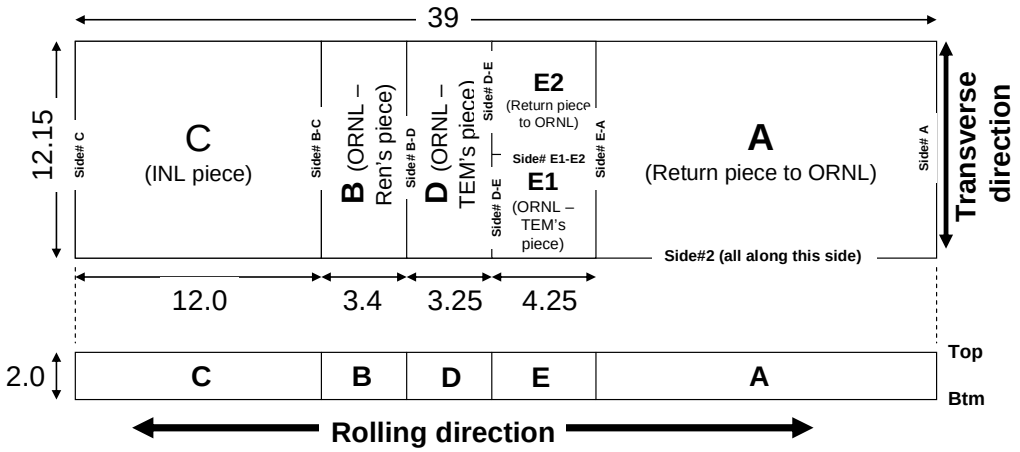

Fig. 17: Cutting plan for CCA Alloy 617 plate

It has been reported that typical Alloy 617 plates delivered by the mill usually contain some clusters of precipitates strung parallel to the rolling direction at certain depth from the surface [11]. Specimen preparation was arranged particularly to characterize the effect, if any, of the precipitates banding as well as rolling direction on mechanical properties. The specimen blanks were cut in both the rolling direction and the transverse direction. Each type of the specimen was machined to cover various directions and depths from the surface. The location and orientation for each specimen cutting was well documented and can be retrieved for future test result analysis if needed. A typical specimen cutting plan for CCA Alloy 617 is presented in Fig. 18 as an example. Two types of specimens, designated as TEM-0007 and WJR-0001, respectively, were machined from the plate. As shown in Fig. 18, both specimen types covered the rolling and transverse directions, as well as the near-surface and near-centerline depths. The SR, MR, ST, and MT stand for surface rolling direction, middle rolling direction, surface transverse direction, and middle transverse direction, respectively. A typical specimen cutting plan for Alloy 230 is given in Fig. 19. Again, each specimen type was cut to cover both rolling and transverse directions.

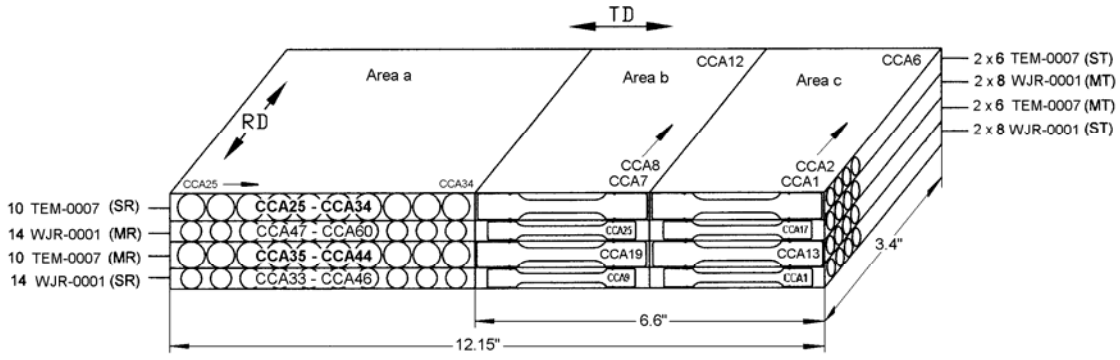

Fig. 18: Cutting plan for creep and tensile specimens from CCA Alloy 617 Plate B

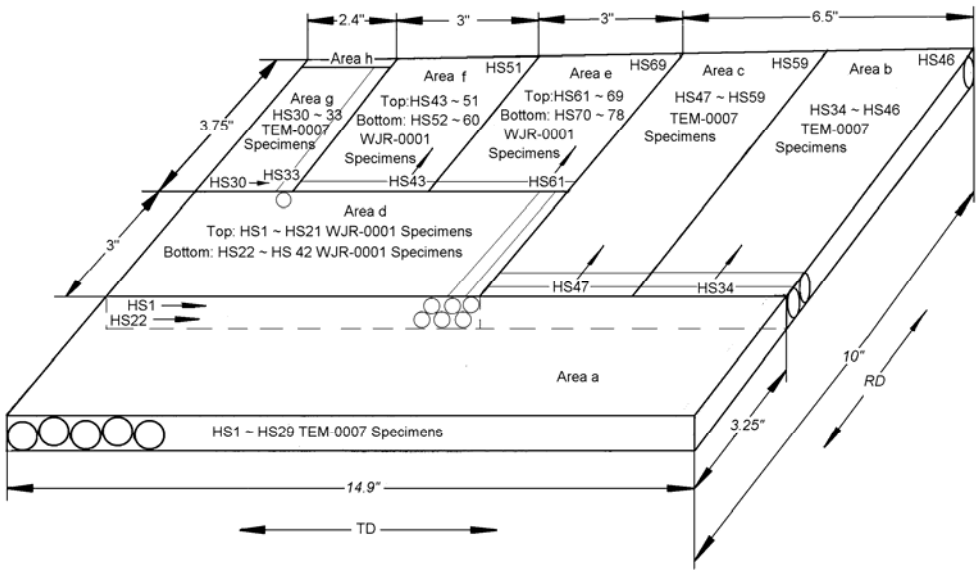

Fig. 19: Cutting plan for creep and tensile specimens from Alloy 230 plate

Three types of specimens were machined for testing and characterization. The TEM-007 specimen, as shown in Fig. 20, was prepared for both creep and tensile tests. The dovetail groves on both shoulders are machined for averaging extensometer to clip on in creep testing. For strain controlled tensile testing, clip type extensometers will be applied directly on gage length punch marks in the reduced section. The WJR-0001 specimens, as shown in Fig. 21, were prepared for creep and tensile tests on post-exposure effects. The small diameter and short total length were designed to enable fitting into a low velocity recirculation helium exposure loop at ORNL for environmental aging before the specimen is ready for creep or tensile testing. The WJR-0002 specimens, as shown in Fig. 22, were prepared for post-exposure fatigue testing. Again, its small size is designed for fitting into the helium environmental aging facility. The

WJR-0002 specimen can be used for fatigue tests under either load or strain control. For strain controlled testing, diametric extensometer will be used.

A dozen CCA 617 TEM-0007 specimens have been received from machine shop for testing. Creep and tensile tests were started upon receiving the specimens. The rest of the specimens will be delivered by the end of August.

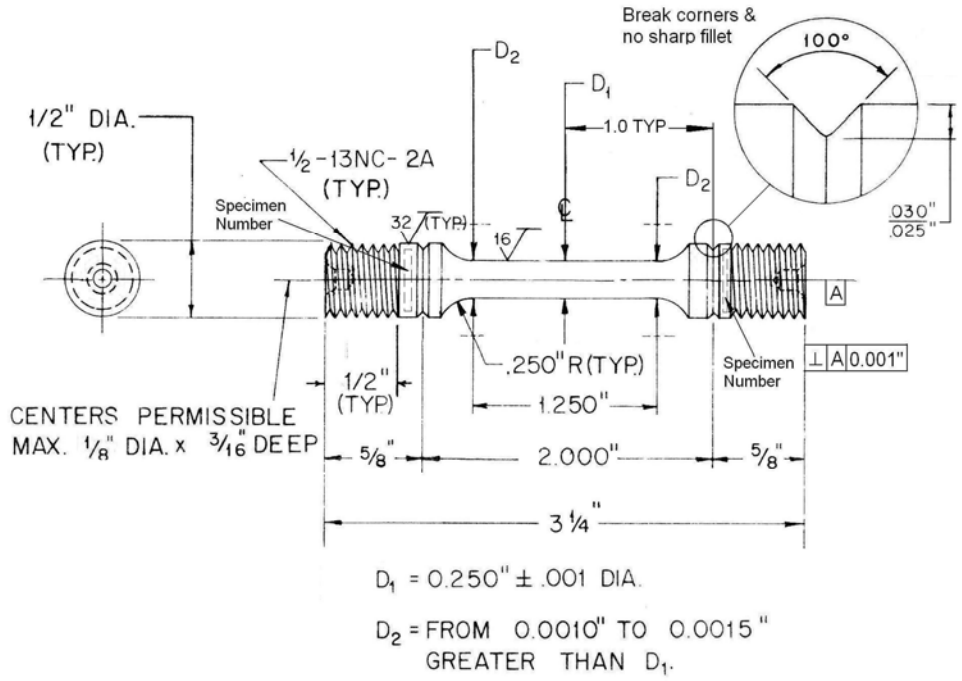

Fig. 20: Tensile and creep specimen TEM-0007

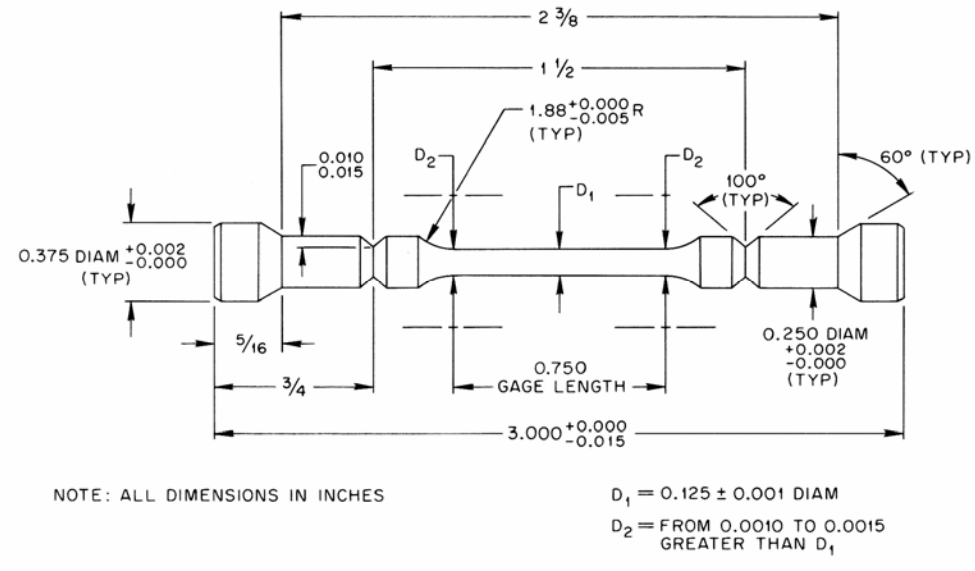

Fig. 21: Tensile and creep specimen WJR-0001 for post exposure study

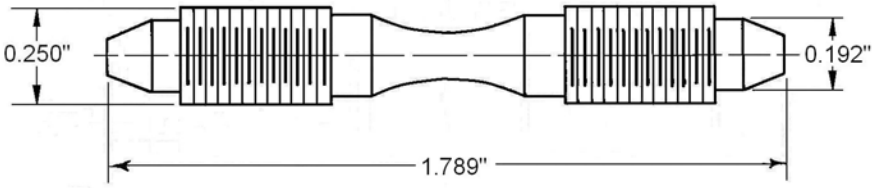

Fig. 22: Fatigue specimen for post exposure study

3.3 Testing Status

One tensile and ten creep testing machines were planned to be refurbished during FY06 for testing CMS Alloy 617 and Alloy 230. The tensile machine is prepared for strain-controlled tensile testing. The machine is a servo-hydraulic MTS 312.21 testing system equipped with a 55.603 kN (12500 lb) load cell. Specimen heating is provided by a 254 mm (10") long split box resistance furnace with seven zones. For testing the tensile specimen which is 82.5 mm (3 ¼") long only the three central zones are employed. Each zone is controlled by its individual Honeywell temperature controller. Because literature review indicates that Alloy 617 becomes highly sensitive to loading rates at the high temperature range of interest to VHTR applications [12], the tensile testing is designed to investigate the loading rate sensitivity of CCA Alloy 617 at high temperatures and provide data for reactor component design model development. To accurately capture the stress-strain curve with as great a strain as possible at various loading rates and temperatures, two extensometers are employed, each on opposite side of the specimen through the side slots of the split resistance furnace. Both extensometers have a 25.4 mm (1") gage length. The first extensometer is an Epsilon strain extensometer with a ±10% strain measuring range at high resolution; and the second one is a modified MTS extensometer with a 0 ~ 100% strain measuring range at a relatively lower resolution. During a test, the first extensometer is used to catch the low strain portion of the stress-strain curve. When the strain accumulates to exceed its maximum measuring range, the second extensometer is used to record the high strain portion of the curve. This would provide more accurate data for modeling purposes than the cross-head displacement normally used for high strain range measurements. A specimen with the extensometer setup is shown in Fig. 23. The test system is controlled using MTS TestStar^{TM} IIs software and all the signals including temperature, load and strain are collected electronically into computer hard drive in a text file for data processing.

The strain-controlled tensile testing is underway. The testing system has demonstrated satisfactory performance. Typical stress-strain curves generated are presented in Fig. 24. More tests will be conducted as the specimens are received from the machine shop.

For creep testing in air environment, as many as 10 lever arm creep machines as shown in Fig. 25 are planned for refurbishment, time and funding permitting. All of the machines have

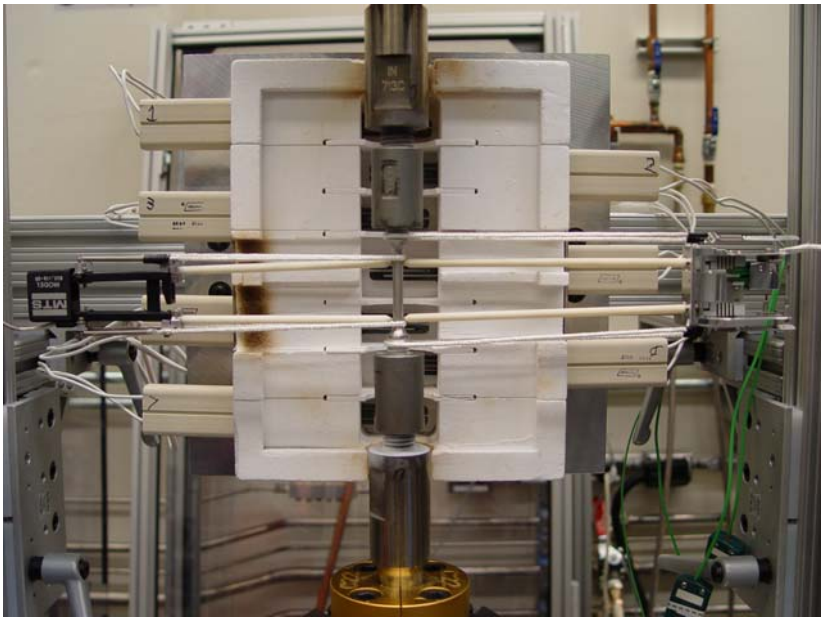

Fig. 23: Experimental setup for strain-controlled tensile testing

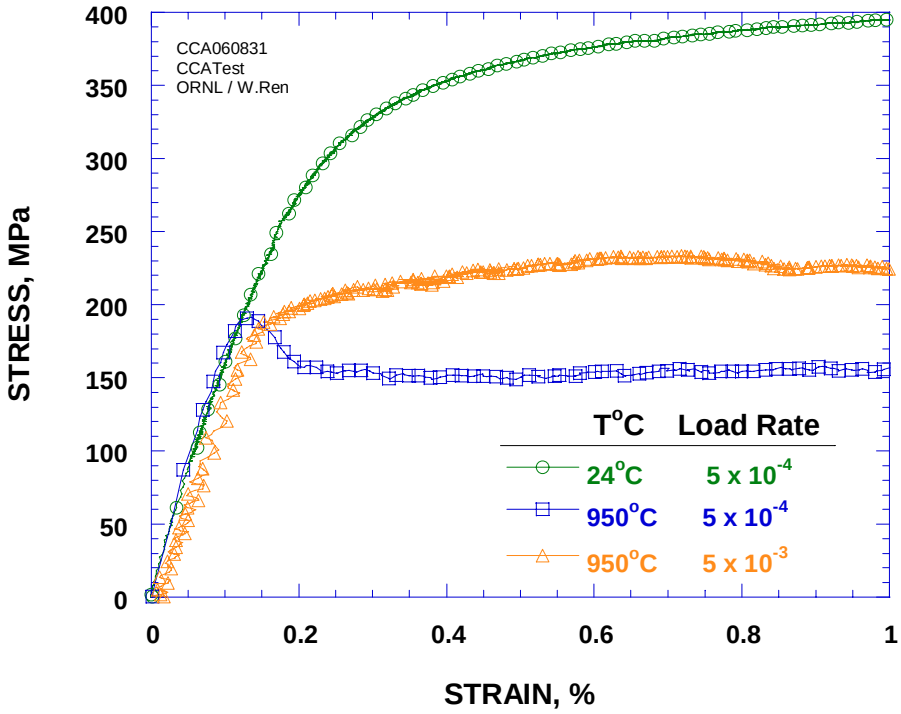

Fig. 24: Strain-controlled tensile test curves at 24 and 950ºC (75 and 1742ºF) and different loading rates

Fig. 25: Ten lever arm creep machines refurbished for testing CMS Alloy 617 and Alloy 230 in air environment

an arm ratio of 1:12 and are refurbished with both K and S type thermocouple capabilities. As stipulated in the test plan [8], creep data in the temperature range of 400ºC (752ºF) to 50ºC (122ºF) higher than the intended application temperature should be provided for codification in ASME B&PV Code Section III Division I Subsection NH. For data gap filling and existing data verification, the testing requires coverage of a very wide temperature and loading range. With both K and S type thermocouple wiring, these 10 machines can cover the entire temperature range needed for Subsection NH. For very high temperature and low load testing, the lever arm will be fixed to test the specimen in a dead-load mode. At present, only short-term tests are conducted to ensure a high machine turnover rate and provide machine downtime for system fine-tuning and adjustments if needed. Long-term tests will be started later in FY07. All the raw test data will be processed, analyzed, compiled, approved, and stored into the Gen IV Materials Handbook [13 -16].

A typical creep curve of CCA Alloy 617 is presented in Fig. 26. As observed in the figure, the alloy seems to exhibit no primary creep but deforms directly into secondary and tertiary creep. However, a close observation as shown in Fig. 27 reveals that limited primary creep still exists in the material. Based on experience from other alloys, primary creep usually becomes more obvious in low load long-term tests. This will be examined when long-term creep tests are conducted in FY07.

Testing on Alloy 230 will be started as soon as the specimens are received from the machine shop by the end of August. The specimen machining activity was told to stop when a Gen IV Program managerial decision to cancel the investigation on Alloy 230 was under consideration after the INL NGNP Materials Workshop in Salt Lake City in June 2006. The machining was recently resumed after the issue was clarified by the management. As mentioned previously,

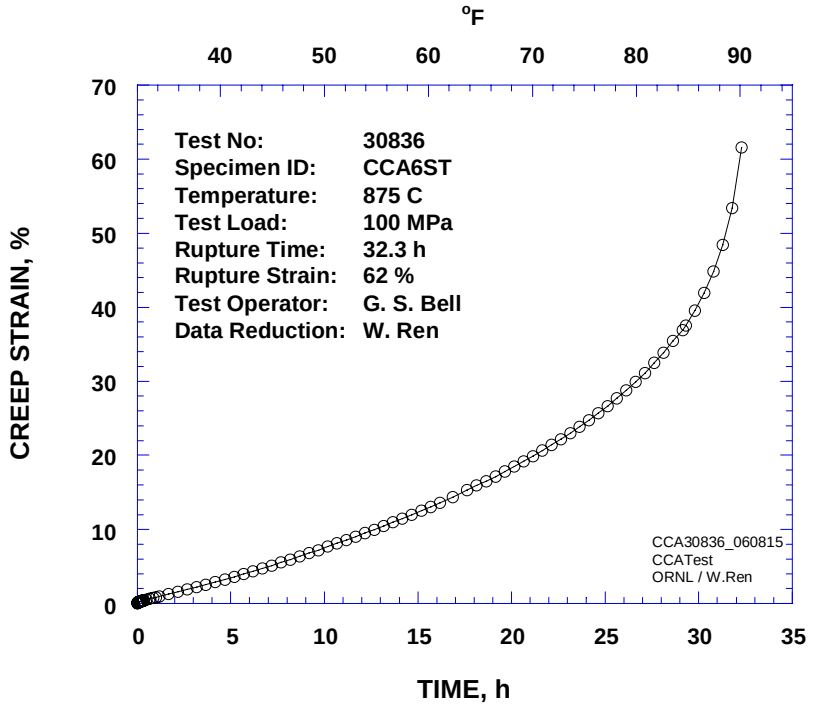

Fig. 26: Typical creep curves of CCA Alloy 617 tested in air environment

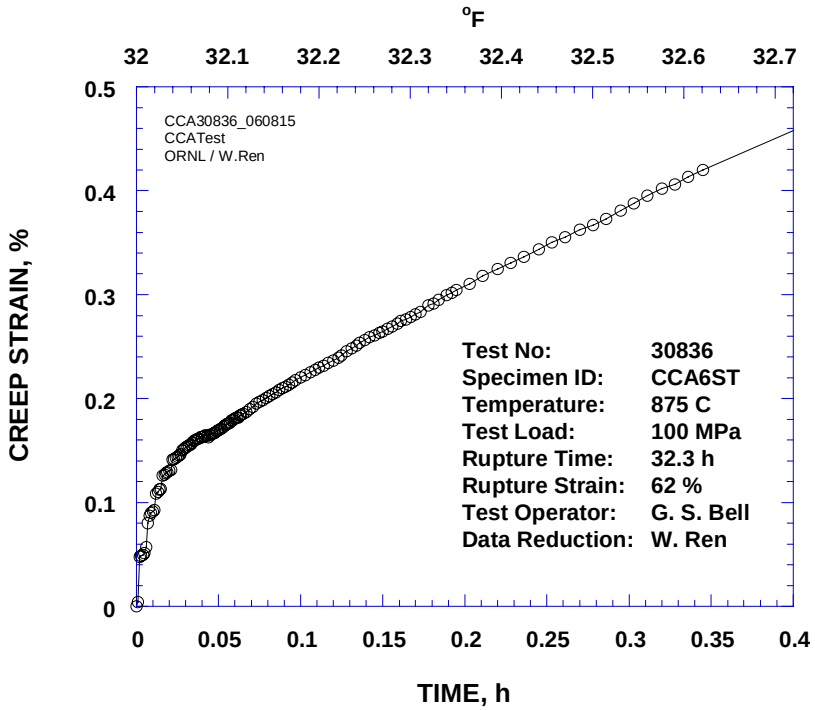

Fig. 27: Limited primary creep of CMS Alloy 617 tested in air environment

Alloy 230 is a relatively new material and lack the abundance of known existing data compared to Alloy 167. Therefore, significant efforts have been made in FY06 to search and collect existing data of Alloy 230 in order to save testing funds and time. Up to date, a total of 299* creep and tensile raw test data curves for Alloy 230 have been collected, which include creep test times up to 28,391 hours and temperatures up to 1149ºC (2100ºF). This will not only save the Gen IV Program several years' worth of testing funds and time on Alloy 230, but also provide guidance for further investigation and data generation on the alloy. Summaries of the creep and tensile data are presented in Table 7 and Table 8, respectively. Because these data were recorded graphically without an electronic version, they must be digitized, edited, compiled, and analyzed in FY07; and their pedigree information will be further searched and collected for Gen IV Materials Handbook input. A typical short-term creep curve of Alloy 230 has been digitized and is presented in Fig. 28. Similar to the CCA Alloy 617 short-term creep curve presented in Fig. 26, no primary creep can be observed in Fig. 28. The original data file provided two curves for the same test. Fig. 28 presents the whole curve at low resolution, and Fig. 29 shows the initial creep curve at high resolution. Analysis indicates that the tow curves do not closely match at the junction point. Some recording error obviously occurred. Verification tests will be conducted when the machined specimens are received from the machine shop.

* Note: The collected raw test data on Alloy 230 include creep curves and tensile test data recorded on grid paper contained in a large box. More than 800 creep curves were inadvertently reported, and the number was use in a previous briefing. Later counting indicates 263 creep curves and 36 tensile datasets actually contained.

Table 7a: Summary of creep test data on Alloy 230

Test No.	Time	Temperature		Stress	
	h	ºC	ºF	MPa	psi
4750	233.3	927	1700	55	8000
4764	249.9	927	1700	55	8000
5418	257.7	760	1400	97	14,000
5424	832.1	871	1600	41	6000
5425	1413.4	871	1600	41	6000
5426	477.2	982	1800	17	2500
5427	401.2	982	1800	17	2500
5428	232.4	649	1200	359	52,000
5429	203.2	649	1200	359	52,000
5441	169	760	1400	97	14,000
5444	2018.6	649	1200	248	36,000
5450	141.8	649	1200	379	55,000
5451	527.4	649	1200	310	45,000
5454	468.3	982	1800	28	4000
5455	79.5	760	1400	193	28,000
5456	599.1	760	1400	138	20,000
5461	1090.7	760	1400	138	20,000
5465	410	982	1800	28	4000
5478	93.7	760	1400	193	28,000
5490	1828.4	871	1600	55	8000
5491	1368.4	871	1600	55	8000
5498	200.7	871	1600	83	12,000
5500	234.4	871	1600	83	12,000
5697	24.5	760	1400	207	30,000
5699	74.8	760	1400	172	25,000
5707	24.9	760	1400	207	30,000
5716	52	760	1400	207	30,000
5725	45	760	1400	207	30,000
5729	60.5	760	1400	172	25,000
5744	627.4	760	1400	138	20,000
5752	29.9	871	1600	97	14,000
5757	32.4	871	1600	97	14,000
5766	219.4	871	1600	69	10,000
5768	224.8	871	1600	69	10,000
5795	73.3	760	1400	172	25,000

Table 7b: Summary of creep test data on Alloy 230

Test No.	Time	Temperature		Stress	
	h	ºC	ºF	MPa	psi
5799	67	760	1400	172	25,000
5800	42.7	871	1600	97	14,000
5814	666.2	760	1400	138	20,000
5815	32	871	1600	97	14,000
5816	278.7	871	1600	69	10,000
5823	247.1	871	1600	69	10,000
5824	425.5	871	1600	41	6000
5827	156.5	760	1400	172	25,000
5829	67.4	871	1600	55	8000
5830	67.1	871	1600	55	8000
5832	165.1	760	1400	172	25,000
5833	424.1	871	1600	41	6000
5834	255.8	871	1600	55	8000
5835	935.7	982	1800	21	3000
5840	113.3	760	1400	117	17,000
5841	87	760	1400	117	17,000
5842	184.2	871	1600	55	8000
5843	40.9	760	1400	117	17,000
5845	111.6	760	1400	103	15,000
5847	115.2	760	1400	103	15,000
5851	86	760	1400	103	15,000
5853	75.1	871	1600	97	14,000
5855	113.6	760	1400	103	15,000
5858	23.7	760	1400	207	30,000
5861	74.8	871	1600	97	14,000
5863	272.9	760	1400	138	20,000
5866	24.2	760	1400	207	30,000
5869	259.6	760	1400	138	20,000
5872	928.3	871	1600	41	6000
5881	208.1	760	1400	138	20,000
5882	40	760	1400	117	17,000
5886	145.5	760	1400	138	20,000
5889	64.3	760	1400	117	17,000
5892	38.1	760	1400	117	17,000
5894	43	982	1800	21	3000

Table 7c: Summary of creep test data on Alloy 230

Test No.	Time	Temperature		Stress	
	h	ºC	ºF	MPa	psi
5897	87	982	1800	41	6000
5898	50.7	760	1400	207	30,000
5899	49.9	760	1400	207	30,000
5900	1065.4	982	1800	21	3000
5901	135.2	760	1400	172	25,000
5904	732.8	760	1400	200	29,000
5910	125.6	760	1400	172	25,000
5911	575.1	760	1400	138	20,000
5913	94.3	982	1800	41	6000
5917	64.8	760	1400	117	17,000
5920	77.2	982	1800	41	6000
5923	88.6	760	1400	117	17,000
5927	115.8	760	1400	103	15,000
5930	114	760	1400	103	15,000
5931	80.1	982	1800	41	6000
5933	56	871	1600	97	14,000
5946	67.8	871	1600	97	14,000
5947	375.2	982	1800	28	4000
5957	481.9	871	1600	69	10,000
5958	664.3	871	1600	41	6000
5959	551.7	871	1600	69	10,000
5977	495.8	871	1600	41	6000
5980	1087.1	871	1600	69	10,000
5984	372	982	1800	28	4000
5986	343.7	982	1800	28	4000
5993	423.3	982	1800	28	4000
5995	726.3	871	1600	69	10,000
5999	210.7	871	1600	55	8000
6002	69	982	1800	41	6000
6003	776.5	982	1800	21	3000
6004	114.8	871	1600	55	8000
6005	1200.8	871	1600	41	6000
6007	59.3	982	1800	41	6000
6010	264.9	982	1800	28	4000
6012	317.8	982	1800	28	4000

Table 7d: Summary of creep test data on Alloy 230

Test No.	Time	Temperature		Stress	
	h	ºC	ºF	MPa	psi
6015	706.5	982	1800	21	3000
6024	771.3	982	1800	21	3000
7129	7200	816	1500	63	9200
7134	11,854.80	871	1600	28	4000
7135	6400	927	1700	19	2800
7136	9824.5	982	1800	12	1700
7238	6185	760	1400	107	15,500
7268	4997.3	760	1400	69	10,000
7271	1968.6	816	1500	62	9000
7272	3497	760	1400	76	11,000
7276	1825.4	982	1800	14	2000
7280	6115.1	982	1800	9	1300
7285	5937.6	760	1400	110	16,000
7287	1143.7	760	1400	90	13,000
7294	785.8	871	1600	48	7000
7297	146.1	982	1800	34	5000
7306	269.9	982	1800	28	4000
7434	1144	704	1300	207	30,000
7443	238.2	760	1400	172	25,000
7456	434.5	760	1400	159	23,000
7473	263.7	760	1400	97	14,000
7480	694.1	704	1300	145	21,000
7502	654.2	927	1700	52	7500
7503	595	704	1300	221	32,000
7507	1583.8	704	1300	117	17,000
7542	1406	760	1400	145	21,000
7545	43.5	927	1700	41	6000
7556	2010.4	927	1700	30	4300
7574	10,854.50	871	1600	43	6300
7575	11,857.00	760	1400	103	15,000
7576	9035	927	1700	22	3200
7577	10,294.80	816	1500	68	9800
7578	9152.5	760	1400	99	14,400
7579	285.4	982	1800	38	5500
7580	734.1	871	1600	76	11,000

Table 7e: Summary of creep test data on Alloy 230

Test No.	Time	Temperature		Stress	
	h	ºC	ºF	MPa	psi
7596	588.7	982	1800	31	4500
7611	3035.5	871	1600	62	9000
7612	1484.9	871	1600	52	7500
7618	4614	968	1775	14	2000
7627	7756.4	913	1675	25	3600
7649	1507.9	982	1800	23	3300
7663	9265.5	760	1400	62	9000
7672	5771.3	968	1775	15	2200
7677	1351.7	913	1675	45	6500
7696	6500	857	1575	45	6500
7742	2091.7	982	1800	21	3000
7758	2175.7	982	1800	15	2200
7762	1553	927	1700	34	5000
7827	560.3	816	1500	114	16,500
7828	3380.6	816	1500	66	9500
7843	236.8	760	1400	103	15,000
7848	7678.5	760	1400	110	16,000
7849	17,721.10	871	1600	41	6000
7854	211.1	982	1800	34	5000
7864	1107.8	982	1800	21	3000
7869	424.9	704	1300	159	23,000
7872	729.6	982	1800	26	3700
7881	810.6	982	1800	14	2000
7895	6546.1	816	1500	76	11,000
7896	2112.1	816	1500	93	13,500
7920	13,860.20	816	1500	72	10,500
7941	168.5	927	1700	62	9000
7950	503.8	927	1700	48	7000
7978	11,962.70	927	1700	14	2100
7983	1050.6	927	1700	39	5700
7995	89.6	927	1700	48	7000
7996	65.4	927	1700	48	7000
7997	89.8	927	1700	48	7000
7998	65.9	927	1700	48	7000
8000	65.5	927	1700	48	7000

Table 7f: Summary of creep test data on Alloy 230

Test No.	Time	Temperature		Stress	
	h	ºC	ºF	MPa	psi
8001	65.8	927	1700	48	7000
8002	20.2	927	1700	48	7000
8003	256.7	927	1700	48	7000
8005	22	927	1700	48	7000
8006	82.7	927	1700	48	7000
8022	89.4	927	1700	41	6000
8032	41.3	927	1700	48	7000
8036	15.3	927	1700	48	7000
8045	64.4	927	1700	48	7000
8079	23	927	1700	48	7000
8080	40.5	927	1700	48	7000
8127	1262.3	1038	1900	12	1700
8128	144.5	927	1700	48	7000
8145	5589.1	982	1800	14	2000
8156	24.4	927	1700	48	7000
8157	312	927	1700	48	7000
8160	69.5	927	1700	48	7000
8161	282.4	927	1700	48	7000
8163	234.4	927	1700	48	7000
8178	4848.4	649	1200	138	20,000
8185	1056.5	816	1500	44	6400
8186	No Data	816	1500	46	6600
8193	1523.3	982	1800	22	3200
8195	167.3	927	1700	62	9000
8199	692.1	704	1300	207	30,000
8204	91.4	816	1500	138	20,000
8209	125	704	1300	276	40,000
8210	427.6	1038	1900	16	2300
8211	1397.9	927	1700	41	6000
8215	1705	649	1200	276	40,000
8218	1116.4	816	1500	97	14,000
8220	No Data	816	1500	66	9500
8221	No Data	704	1300	138	20,000
8226	65.2	927	1700	48	7000
8227	233.7	927	1700	48	7000

Table 7g: Summary of creep test data on Alloy 230

Test No.	Time	Temperature		Stress	
	h	ºC	ºF	MPa	psi
8228	114.7	1038	1900	24	3500
8233	342.4	649	1200	310	45,000
8235	493.7	982	1800	31	4500
8236	44.7	927	1700	48	7000
8237	40.7	927	1700	48	7000
8238	4264	704	1300	159	23,000
8259	3443.9	649	1200	241	35,000
8269	28,391.40	816	1500	59	8500
8301	115	1093	2000	14	2000
8302	234.9	1093	2000	10	1500
8303	2378.4	1093	2000	6	800
8304	4352.4	1093	2000	4	600
8336	39.5	1149	2100	10	1500
8337	165.6	1149	2100	7	1000
8338	2212	1149	2100	3	500
8512	179.6	927	1700	41	6000
8516	165.2	927	1700	41	6000
8524	187.9	927	1700	41	6000
8533	36.7	927	1700	62	9000
8536	25.8	927	1700	62	9000
8539	139.4	927	1700	41	6000
8542	29.6	927	1700	62	9000
8543	266.8	927	1700	41	6000
8544	123.6	927	1700	41	6000
8546	111.3	927	1700	41	6000
8548	34.2	927	1700	62	9000
8559	22.3	927	1700	62	9000
8560	184	927	1700	41	6000
8562	116.5	927	1700	41	6000
8563	145.3	927	1700	41	6000
8564	31.5	927	1700	62	9000
8569	44.7	927	1700	62	9000
8570	59	927	1700	62	9000
8588	1370.2	1093	2000	7	1000
8610	29.9	982	1800	55	8000

Table 7h: Summary of creep test data on Alloy 230

Test No.	Time	Temperature		Stress	
	h	ºC	ºF	MPa	psi
8615	1132.7	982	1800	22	3200
8626	76.8	816	1500	145	21,000
8643	26,225.00	760	1400	86	12,500
8664	2053	593	1100	448	65,000
8665	38.1	593	1100	552	80,000
8666	1948.9	649	1200	276	40,000
8667	215.2	649	1200	379	55,000
8668	18.2	649	1200	483	70,000
8670	531.9	760	1400	159	23,000
8671	111.9	760	1400	200	29,000
8672	333.6	816	1500	117	17,000
8673	51.8	816	1500	159	23,000
8675	57.1	871	1600	110	16,000
8676	843.6	927	1700	48	7000
8677	33.5	927	1700	83	12,000
8693	121	927	1700	69	10,000
8715	1998.8	1038	1900	10	1500
8800	10,672.20	1038	1900	8	1100

Table 8: Summary of tensile test data on Alloy 230

Test No	Sample	Temperature		Modulus		UTS		0.2% YS		El.	RA
	ID	ºC	ºF	GPa	x10^6 psi	MPa	ksi	MPa	ksi	%	%
T-123893	1	24	75	237.71	34.5	861.3	125	368.6	53.5	54	49
T-123894	2	24	75	228.75	33.2	861.3	125	389.3	56.5	53	47
T-123901	3	93	200	201.19	29.2	813.0	118	354.8	51.5	53	48
T-123902	4	93	200	188.10	27.3	813.0	118	358.3	52.0	53	48
T 123903	5	149	300	190.16	27.6	785.5	114	313.5	45.5	54	48
T-123904	6	149	300	203.94	29.6	778.6	113	306.6	44.5	53	47
T-123905	7	204	400	214.28	31.1	764.8	111	285.9	41.5	52	48
T-123906	8	204	400	192.23	27.9	757.9	110	305.9	44.4	51	46
T-123907	9	260	500	212.21	30.8	757.9	110	291.4	42.3	51	47
T-123908	10	260	500	199.12	28.9	751.0	109	273.5	39.7	53	46
T-123913	11	316	600	190.85	27.7	744.1	108	278.4	40.4	54	47
T-123914	12	316	600	208.77	30.3	751.0	109	297.6	43.2	56	46
T-123915	13	371	700	183.27	26.6	744.1	108	277.0	40.2	55	47
T-123916	14	371	700	208.77	30.3	737.2	107	296.3	43.0	53	48
T-123917	15	427	800	192.92	28.0	744.1	108	270.8	39.3	55	49
T-123918	16	427	800	221.17	32.1	730.3	106	286.6	41.6	56	48
T-123919	17	482	900	196.37	28.5	723.5	105	259.1	37.6	54	50
T-123920	18	482	900	192.92	28.0	723.5	105	255.6	37.1	56	47
T-123929	19	538	1000	179.14	26.0	716.6	104	258.4	37.5	56	48
T-123030	20	538	1000	179.14	26.0	709.7	103	283.2	41.1	55	47
T-123931	21	593	1100	189.48	27.5	702.8	102	248.0	36.0	58	49
T-123932	22	593	1100	192.23	27.9	689.0	100	247.4	35.9	60	49
T-123933	23	649	1200	167.43	24.3	678.7	98.5	242.5	35.2	59	49
T-123934	24	649	1200	191.54	27.8	675.2	98.0	234.9	34.1	59	50
T-123935	25	704	1300	183.96	26.7	609.8	88.5	257.7	37.4	78	48
T-123936	26	704	1300	172.25	25.0	620.1	90.0	251.5	36.5	70	49
T-123945	27	760	1400	158.47	23.0	523.6	76.0	265.3	38.5	71	55
T-123946	28	760	1400	163.29	23.7	520.2	75.5	255.6	37.1	73	57
T-123947	29	816	1500	152.96	22.2	410.0	59.5	263.2	38.2	60(a)	60
T-123948	30	816	1500	147.45	21.4	410.0	59.5	217.7	31.6	64(a)	64
T-123962	31	871	1600	152.96	22.2	305.2	44.3	195.7	28.4	65(a)	70
T-123963	32	871	1600	171.56	24.9	304.5	44.2	203.9	29.6	72(a)	72
T-123964	33	927	1700	137.11	19.9	222.5	32.3	137.8	20.0	64(a)	76
T-123965	34	927	1700	143.31	20.8	222.5	32.3	137.8	20.0	58(a)	75
T-123895	35	982	1800	124.71	18.1	164.0	23.8	98.5	14.3	73(a)	72
T-123896	36	982	1800	119.20	17.3	158.5	23.0	97.1	14.1	70(a)	73

(a) Specimen failed outside gage mark; value based on overall length measurements.

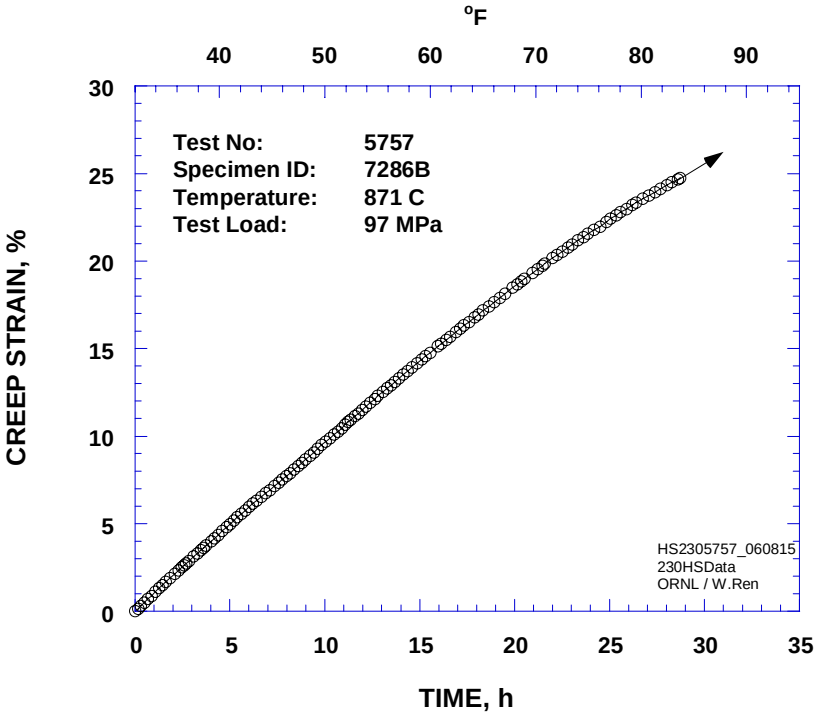

Fig. 28: Typical creep curve of Alloy 230 tested in air environment

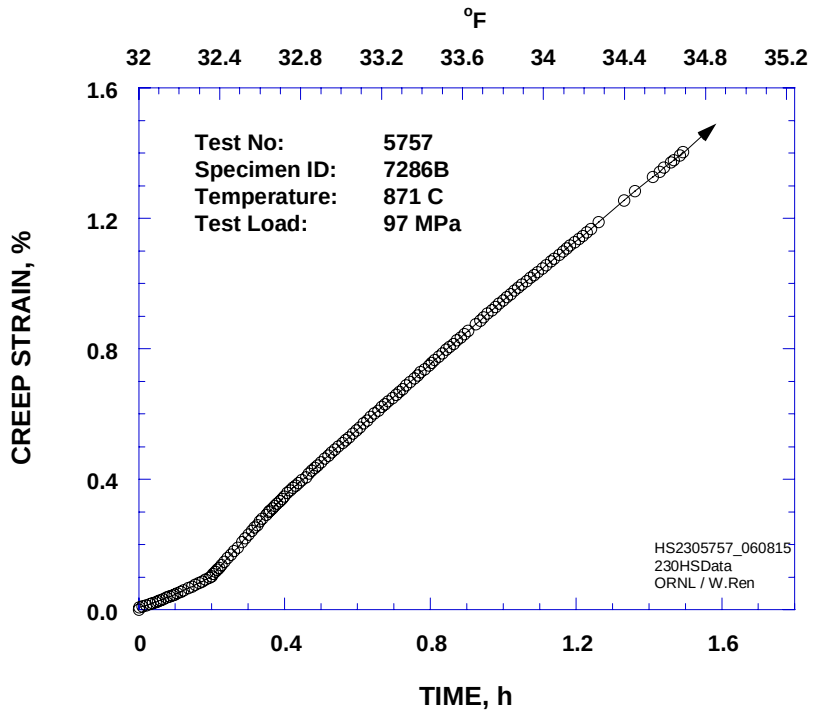

Fig. 29: Initial portion of the creep curve in Fig. 28

4. CREEP-FATIGUE TESTING OF STANDARD CHEMISTRY ALLOY 617 AT INL (T. Totemeier & D. Clark)

4.1 Material and Test Procedures

Tests were performed on specimens machined from the 20 mm thick plate obtained in FY04. The plate was commercially procured from Special Metals Corporation meeting ASTM specification B 168-01. A description of the plate and its basic characteristics was presented in Ref. [17]. Table 9 lists the manufacturer-certified chemical composition. Cylindrical creep-fatigue specimens with 6.4 mm gage diameter and 20 mm reduced section were machined from the plate for testing; the long axes of the specimens were aligned with the plate rolling direction. Low-stress grinding and longitudinal polishing were used in the final machining of the reduced section to eliminate cold work and circumferential machining marks.

Table 9: Standard chemistry Alloy 617 chemical composition

Heat	Composition (wt.%)											
	Ni	Cr	Co	Mo	Fe	Al	Ti	C	Mn	Si	S	B
XX2834UK	Bal.	21.91	11.42	9.78	1.69	0.96	0.34	0.08	0.11	0.12	0.001	0.002

Creep-fatigue tests were also performed on specimens with fusion welds. The specimens were machined from the welded plates described in Ref. [17, 18]. As described in the reports, butt joints were created in the plates by a gas-tungsten arc process with Alloy 617 filler wire. Cross-weld test specimens were machined from the welded plates as shown schematically in Fig. 30. The reduced test section contained base metal, heat-affected zone (HAZ), and weld metal. A slightly different specimen geometry was used for the weldment specimens (8.5 mm gage diameter and 33.5 mm reduced section) for testing on a different load frame. A limited set of comparison tests were performed on base metal specimens to confirm that fatigue life was not significantly affected by the difference in specimen geometry or load frame; no differences were observed.

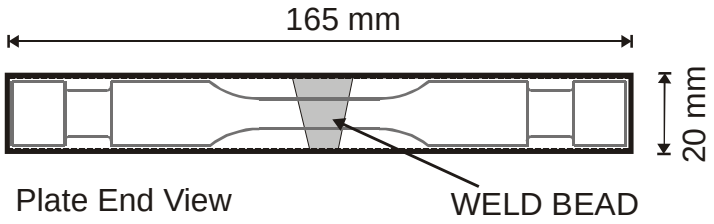

Fig. 30: Schematic diagram showing orientation of creep-fatigue specimen with respect to welded plate

Creep-fatigue tests were performed on MTS servo-hydraulic test machines in total axial strain control. Strains were fully reversed (R = –1). Tests were performed at temperatures of 800 and 1000°C (1427 and 1832ºF) and total strain ranges from 0.3% to 1.0%. Depending on the test machine, specimens were heated either using a resistance furnace or by induction. Type

K or S thermocouples were spot-welded or wired to the specimen surface to monitor specimen temperature.

The test waveform was trapezoidal with a ramp rate of 1 x 10^{-3} sec^{-1}, and creep was introduced by a hold period at the maximum tensile strain which varied from 0 (continuous cycling) to 1800 s. Tests were terminated when the peak tensile load had dropped by approximately 60% of the initial, stable value (generally achieved after 20 cycles). Testing did not cause specimen separation; specimens were usually broken into two halves at room temperature after testing.

Base metal specimens were tested in air, vacuum, and purified Ar environments. Fusion weld specimens were only tested in air. Tests in vacuum and purified Ar were performed on a test machine with a stainless steel environmental chamber, induction heating, and a water-cooled extensometer described in Ref. [19]. A vacuum level of 3 ~ 4 x 10^{-5} Torr was reached during testing. Tests in purified Ar gas were performed at 200 Torr above ambient atmospheric pressure. Standard ultra-high purity Ar was further purified during testing by continuous recirculation through a heated metal getter, either a VICI model HP2 or a SAES model GC50. The recirculation rate was approximately 100 ml/min for the VICI getter and 500 ml/min for the GC50 getter. A test was also performed in static (non-recirculated) Ar that had been passed through the GC50 getter during chamber filling. In all cases the chamber was pumped down to 3x10^{-5} Torr vacuum prior to filling with Ar.

4.2 Results

Tables 10 through 14 list conditions and results for all creep-fatigue tests performed to date. Cycles to initiation and failure were determined after creep-fatigue testing from plots of the ratio of peak tensile to peak compressive load versus cycles. Figs. 31 through 33 show typical variations of peak tensile and compressive stress with cycles for base metal tests at 1000°C (1832ºF) in air at 0.3% and 1.0% strain range, and a test at 1000°C (1832ºF) in vacuum at 1.0% strain range. Similar variations were observed for tests on fusion weldment specimens at 1000°C (1832ºF).

Also shown are plots of the ratio of peak tensile to peak compressive stress versus cycles which were used to deduce cycles to macro-crack initiation and specimen failure. Determination of these values from peak tensile/compressive stress ratio (rather than peak tensile stress or total stress range) allows changes in peak stresses due to cyclic work hardening or softening to be distinguished from those caused by crack formation and propagation, since cracking selectively reduces peak tensile stresses in a strain-controlled test. Crack initiation was defined as the point at which the stress ratio sharply deviated from an initial trend. As shown in Fig. 31, the initial trend for tests at 0.3% strain range with a tensile hold time was a gradual reduction in ratio, while for continuous-cycle tests at 0.3% strain range and all tests at 1.0% strain range the initial stress ratio was constant (Figs. 32 and 33). Failure was defined as a further 20% reduction in stress ratio from the point of crack initiation. In the vacuum example (Fig. 33) cracking did not occur prior to test termination (this was verified metallographically), rather the peak tensile and compressive stresses were sufficiently reduced by decarburization to terminate the test. The fatigue test control and acquisition software determines test termination by drop in peak tensile

Table 10: Creep-fatigue tests of standard chemistry 617 base metal at 800°C in air

Test ID	Total Strain Range (%)	Tensile Hold Time (s)	Stable Maximum Stress (MPa)	Stable Minimum Stress (MPa)	Cycles to Crack Initiation	Cycles to Failure
IN617-STD-800-03	0.3	0	240	-240	N/A*	72500
IN617-STD-800-04	0.3	0	240	-250	28300	29680
IN617-STD-800-14	0.3	0	240	-250	100000	100000
IN617-STD-800-09	0.3	60	210	-280	N/A*	8370
IN617-STD-800-10	0.3	60	180	-300	4000	4760
IN617-STD-800-13	0.3	600	170	-330	1790	3960
IN617-STD-800-17	0.5	0	300	-300	1950	2100
IN617-STD-800-16	0.8	0	330	-340	690	875
IN617-STD-800-01	1.0	0	420	-430	530	690
IN617-STD-800-02	1.0	0	350	-350	775	890
IN617-STD-800-05	1.0	60	410	-440	380	485
IN617-STD-800-06	1.0	60	340	-360	340	440
IN617-STD-800-07	1.0	600	380	-410	300	580
IN617-STD-800-11	1.0	600	400	-440	100	390

* Inconsistent peak load data; not possible to determine initiation point.

Table 11: Creep-fatigue tests of standard chemistry 617 base metal at 1000°C in air

Test ID	Total Strain Range (%)	Tensile Hold Time (s)	Stable Maximum Stress (MPa)	Stable Minimum Stress (MPa)	Cycles to Crack Initiation	Cycles to Failure
IN617-STD-1000-06	0.3	0	160	-160	12700	13610
IN617-STD-1000-06R	0.3	0	160	-170	12880	12930
IN617-STD-1000-12	0.3	18	150	-160	1560	2060
IN617-STD-1000-13	0.3	18	140	-160	2200	2770
IN617-STD-1000-14	0.3	18	120	-120	2020	2420
IN617-STD-1000-07	0.3	60	140	-160	3300	3830
IN617-STD-1000-28	0.3	60	100	-120	4330	5020
IN617-STD-1000-08	0.3	180	130	-160	3330	4010
IN617-STD-1000-08R	0.3	180	140	-160	3100	3530
IN617-STD-1000-09	0.3	600	130	-150	2130	2520
IN617-STD-1000-18B	0.3	600	130	-170	1500	2110
IN617-STD-1000-10	0.3	1800	130	-150	1200	1940
IN617-STD-1000-23	0.3	1800	130	-160	1580	2000
IN617-STD-1000-45	0.5	0	110	-110	2980	3490
IN617-STD-1000-46	0.8	0	110	-110	550	885
IN617-STD-1000-01	1.0	0	160	-160	240	525
IN617-STD-1000-01R	1.0	0	150	-160	195	680
IN617-STD-1000-11	1.0	18	150	-160	145	530
IN617-STD-1000-11R	1.0	18	150	-160	165	510
IN617-STD-1000-02	1.0	60	150	-160	185	415
IN617-STD-1000-21	1.0	60	120	-130	135	370
IN617-STD-1000-03	1.0	180	160	-140	175	360
IN617-STD-1000-03R	1.0	180	150	-150	150	330
IN617-STD-1000-04	1.0	600	150	-160	160	400
IN617-STD-1000-15	1.0	600	140	-150	130	300
IN617-STD-1000-05	1.0	1800	140	-140	220	460
IN617-STD-1000-17	1.0	1800	140	-140	360	460

Table 12: Creep-fatigue tests of standard chemistry Alloy 617 at 1000°C in 3 x 10^{-5} Torr vacuum.

Test ID	Total Strain Range (%)	Tensile Hold Time (s)	Initial[a] Maximum Stress (MPa)	Initial[a] Minimum Stress (MPa)	Cycles to Crack Initiation	Cycles to Failure
IN617-STD-1000-24	0.3	0	130	-130	N/A[b]	~45000
IN617-STD-1000-36	0.3	0	120	-120	13000	16800
IN617-STD-1000-22	0.3	60	120	-130	370	4950
IN617-STD-1000-26[d]	0.3	60	110	-120	4700	5370
IN617-STD-1000-26[e]	0.3	60	110	-120	N/A[c]	> 2350[c]
IN617-STD-1000-26f	0.3	60	110	-120	4560	5310
IN617-STD-1000-29	0.3	600	110	-120	170	1960
IN617-STD-1000-37	0.3	600	110	-130	N/A[c]	> 2450[c]
IN617-STD-1000-41	0.3	600	90	-100	N/A[c]	> 5320[c]
IN617-STD-1000-32	1.0	0	120	-120	N/A[c]	> 1700[c]
IN617-STD-1000-38	1.0	0	110	-110	N/A[c]	> 1700[c]
IN617-STD-1000-42	1.0	0	100	-110	1790	2375
IN617-STD-1000-33	1.0	60	110	-120	670	930
IN617-STD-1000-34	1.0	600	110	-120	N/A[c]	> 590[c]
IN617-STD-1000-35	1.0	600	110	-110	540	1010
IN617-STD-1000-39	1.0	600	110	-120	700	890

a: Continuously decreasing load range – no stabilization.
b: Poor definition of load ratio – unable to determine initiation point.
c. No indication of cracking after testing, cycles to failure represent point of test termination due to 30% drop in load range.
d. Recirculating purified Ar, VICI getter
e. Recirculating purified Ar, SAES getter
f. Static purified Ar, SAES getter

Table 13: Creep-fatigue tests of standard chemistry 617 fusion weld joint at 800°C in air

Test ID	Total Strain Range (%)	Tensile Hold Time (min)	Stable Maximum Stress (MPa)	Stable Minimum Stress (MPa)	Cycles to Crack Initiation	Cycles to Failure
IN617-FUS-800-02	0.3	0	250	-250	9000	9750
IN617-FUS-800-06	0.3	60	200	-300	640	1140
IN617-FUS-800-03	0.3	600	180	-290	780	930
IN617-FUS-800-01	1.0	0	330	-350	380	435
IN617-FUS-800-04	1.0	60	350	-370	130	148
IN617-FUS-800-05	1.0	600	360	-380	83	104

Table 14: Creep-fatigue tests of standard chemistry 617 fusion weld joint at 1000°C in air

Test ID	Total Strain Range (%)	Tensile Hold Time (min)	Stable Maximum Stress (MPa)	Stable Minimum Stress (MPa)	Cycles to Crack Initiation	Cycles to Failure
IN617-FUS-1000-06	0.3	0	120	-110	2040	2890
IN617-FUS-1000-10	0.3	0	130	-130	2270	3280
IN617-FUS-1000-14	0.3	18	110	-110	1100	1570
IN617-FUS-1000-07	0.3	60	110	-120	850	1300
IN617-FUS-1000-11	0.3	60	120	-120	145	1400
IN617-FUS-1000-08	0.3	180	120	-130	10	930
IN617-FUS-1000-09	0.3	600	110	-130	20	430
IN617-FUS-1000-13	0.3	600	100	-110	680	780
IN617-FUS-1000-16	0.3	1800	110	-110	950	1080
IN617-FUS-1000-03	1.0	0	110	-130	200	475
IN617-FUS-1000-17	1.0	0	130	-120	410	530
IN617-FUS-1000-18	1.0	18	130	-120	270	430
IN617-FUS-1000-04	1.0	60	110	-130	160	200
IN617-FUS-1000-19	1.0	60	120	-130	190	270
IN617-FUS-1000-02	1.0	180	110	-120	135	180
IN617-FUS-1000-05	1.0	600	110	-120	50	95
IN617-FUS-1000-20	1.0	600	120	-120	105	160

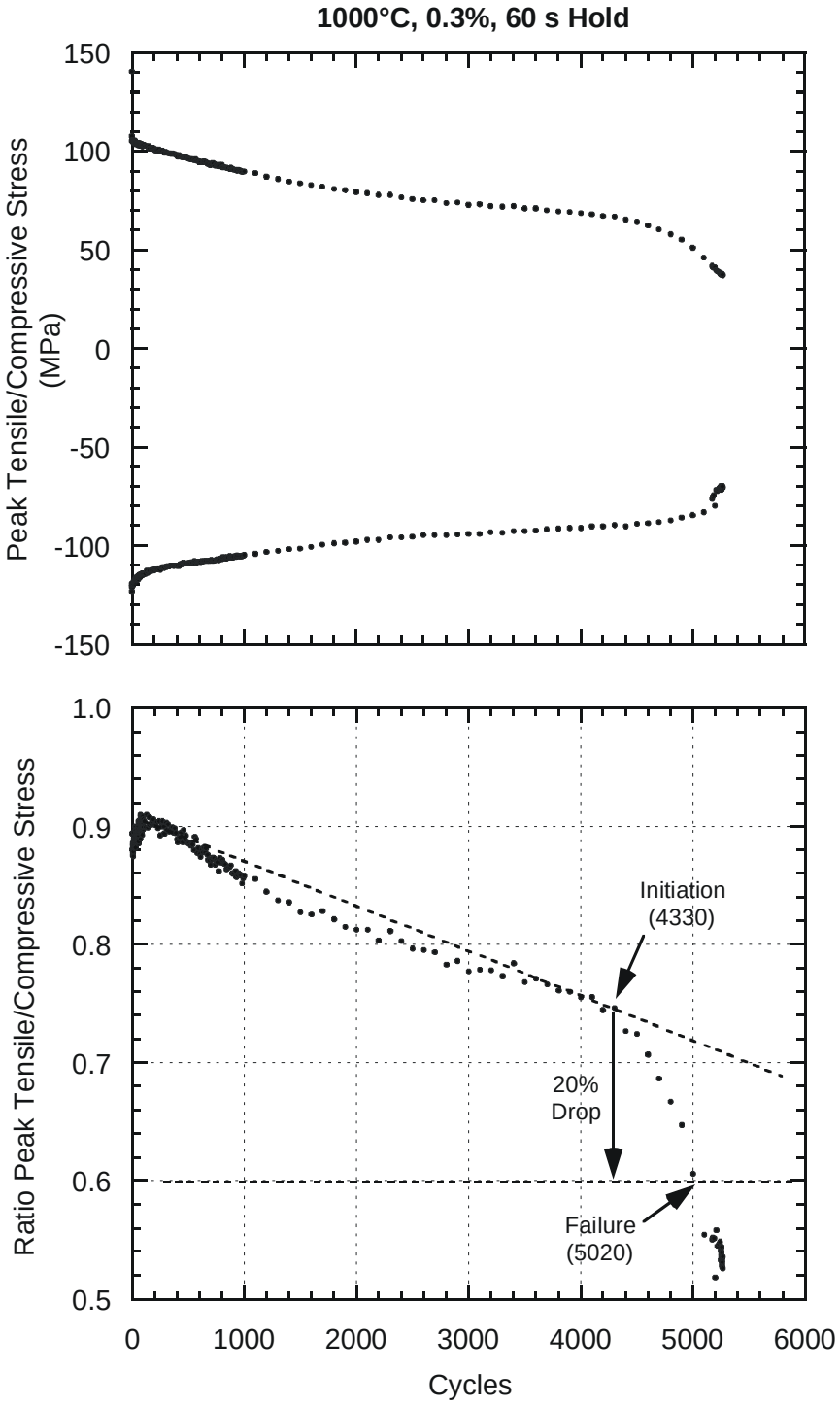

Fig. 31: Peak/valley stress and stress ratio for creep-fatigue test performed in air at 0.3% strain range and 60 s tensile hold.

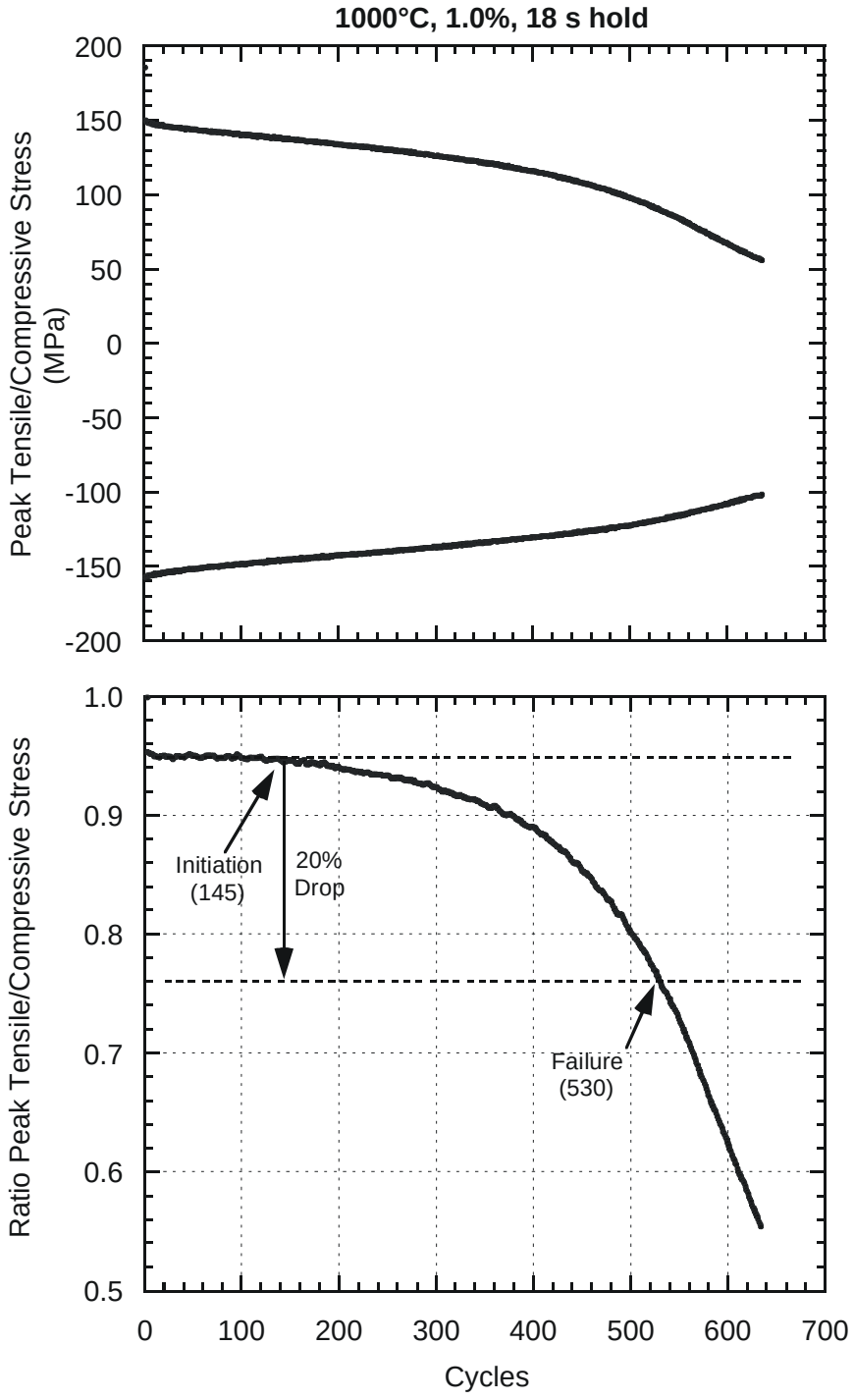

Fig. 32: Peak/valley stress and stress ratio for creep-fatigue test performed in air at 1.0% strain range and 18 s tensile hold.

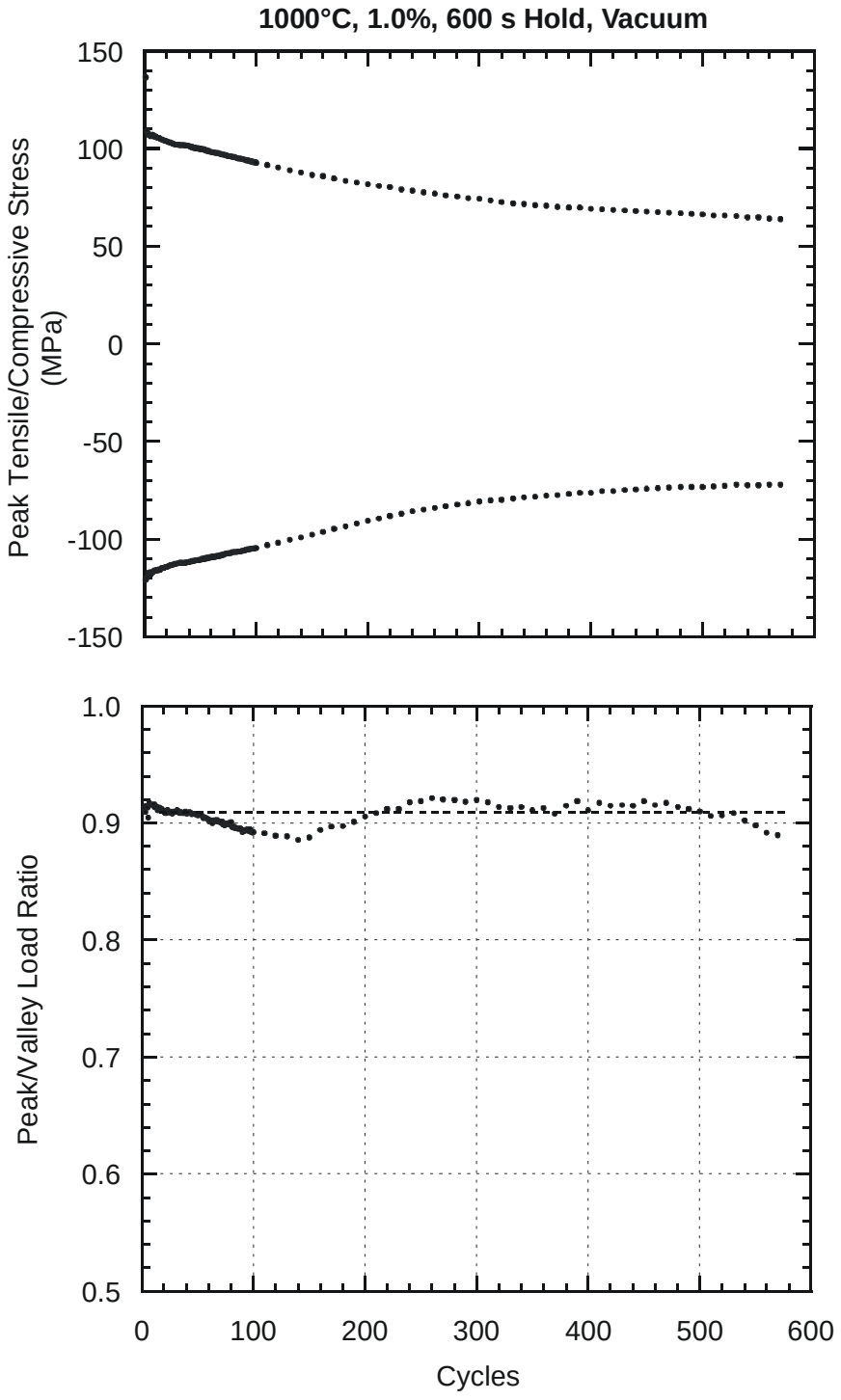

Fig. 33: Peak/valley stress and stress ratio for creep-fatigue test performed in $3x10^{-5}$ Torr vacuum at 1.0% strain range and 600 s tensile hold.

stress only. Several tests in vacuum and purified Ar were terminated prior to cracking in this manner.

As depicted in Figs. 31 through 33, at 1000°C a gradual softening was observed for all test conditions; there typically was no extended period in which the stress range was constant. At 800°C monotonic and cyclic work hardening was observed, as reflected in the differences in stress ranges for strain ranges of 0.3 and 1.0% listed in Table 10. Cyclic work hardening combined with tensile hold periods led to the development of significant compressive mean stresses, as shown in Fig. 34. In addition, marked serrated flow indicative of dynamic strain aging was observed in tests at 800°C.

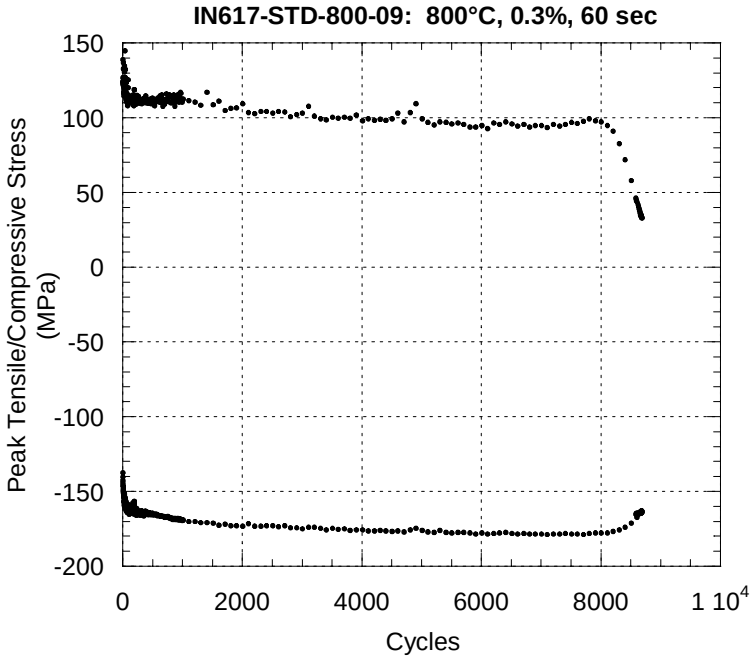

Fig. 34: Peak tensile and compressive stresses for creep-fatigue test performed at 800°C, 0.3% strain range and 60 s tensile hold. A mean compressive stress of 84 MPa developed during the test.

4.2.1 Base Metal - Air

Plots summarizing the creep-fatigue behavior of Alloy 617 base metal in air at 800 and 1000°C (1472 and 1832ºF) are shown in Figs. 35 through 38. The life data at each temperature are depicted in two ways: Figs. 35 and 37 are plots of cycles to failure versus strain range with data from selected hold time tests shown; Figs. 36 and 38 are plots of cycles to failure versus tensile hold time at 0.3 and 1.0% total strain ranges. At both temperatures introducing a tensile hold period reduced the fatigue life; the reductions were more marked at 0.3% total strain range. For the 1.0% strain range at both temperatures the reduction in life due to the tensile hold appeared to saturate with increasing duration. For 0.3% at 800°C (1472ºF) the more limited data

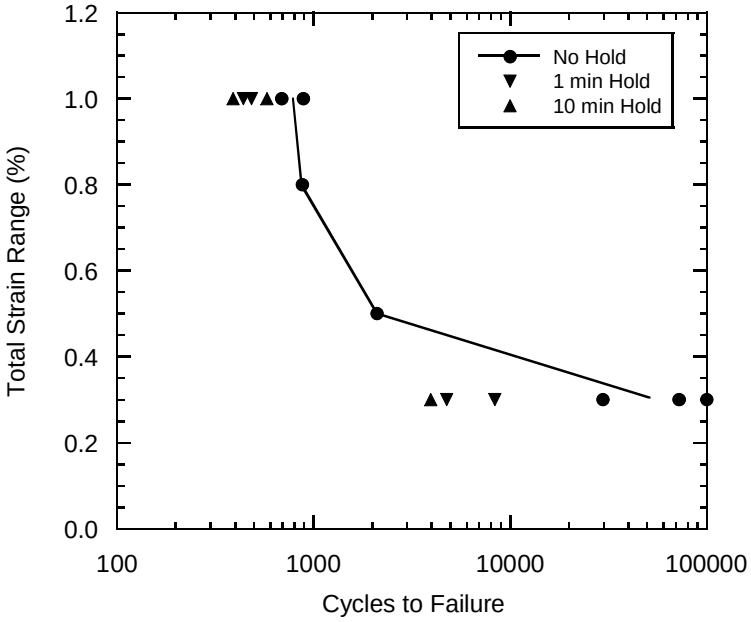

Fig. 35: Cycles to failure versus total strain range for Alloy 617 base metal at 800°C in air.

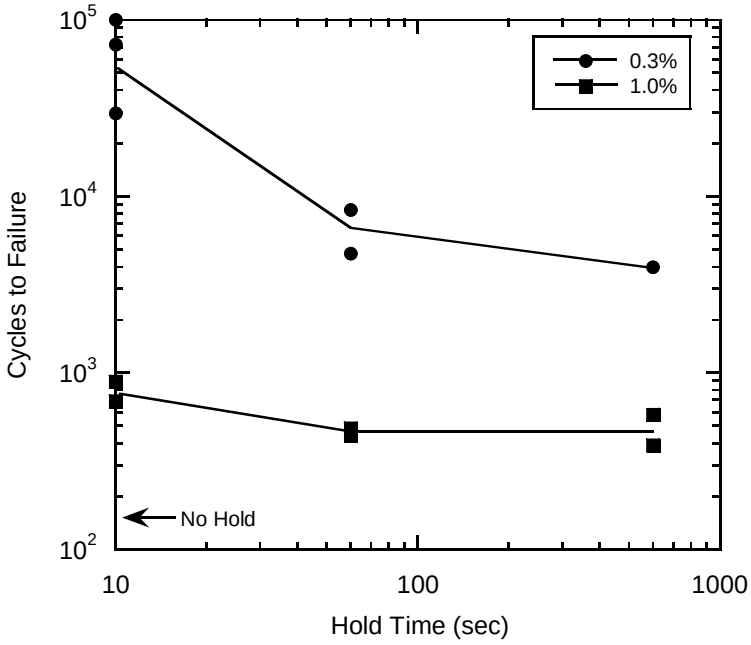

Fig. 36: Cycles to failure versus tensile hold period for Alloy 617 base metal at 800°C in air

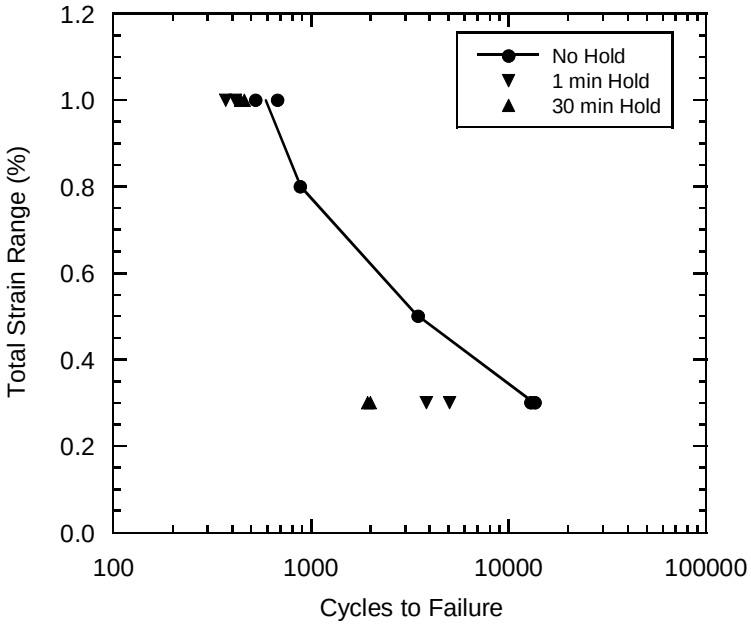

Fig. 37: Cycles to failure versus total strain range for Alloy 617 base metal at 1000°C in air

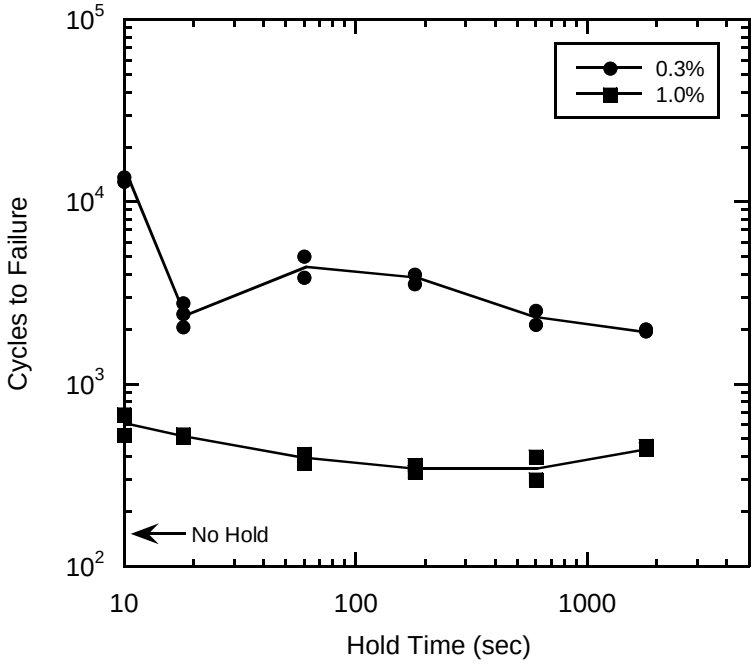

Fig. 38: Cycles to failure versus tensile hold time for Alloy 617 base metal at 1000°C in air

(out to 600 s only) do not indicate saturation. For tests at 0.3% and 1000°C (1832ºF) a minimum in life was observed at 18 s hold time, lives then increased at 60 s hold time and steadily decreased beyond 60 s hold time. The results of repeat tests performed were generally consistent. Creep-fatigue lives at the two temperatures were similar for 1.0% strain range; lives were longer at 800°C (1472ºF) than at 1000°C (1832ºF) for 0.3% strain range. The number of cycles to crack initiation exhibited trends very similar to the number of cycles to failure and are not shown here.

Creep-fatigue cracking in air at 1000°C (1832ºF) was clearly influenced by the oxidizing environment. External oxide scales were observed on all specimens; beneath the external scale a zone of internal oxidation along grain boundaries was present, as shown in Fig. 39. The thickness of the external oxide scale ranged from 1-2 μm for the shortest duration test (1.0% strain range - no hold, 6 hr duration) to approximately 15 μm for a long duration test (1.0% strain range - 1800 s hold, 1000 hr duration). Similarly, internal oxidation depths ranged from 0 to 50 μm. Cracks initiating at oxidized grain boundaries clearly led to failure; a typical secondary crack initiated at surface oxide is also shown in Fig 39. Cavities initiated at carbide particles in stringers were observed for tests with tensile hold periods (Fig 40); high cavity densities were observed ahead of large cracks. The degree of cavitation qualitatively increased with hold time.

Metallographic analysis of creep-fatigue specimens tested at 800°C is in progress.

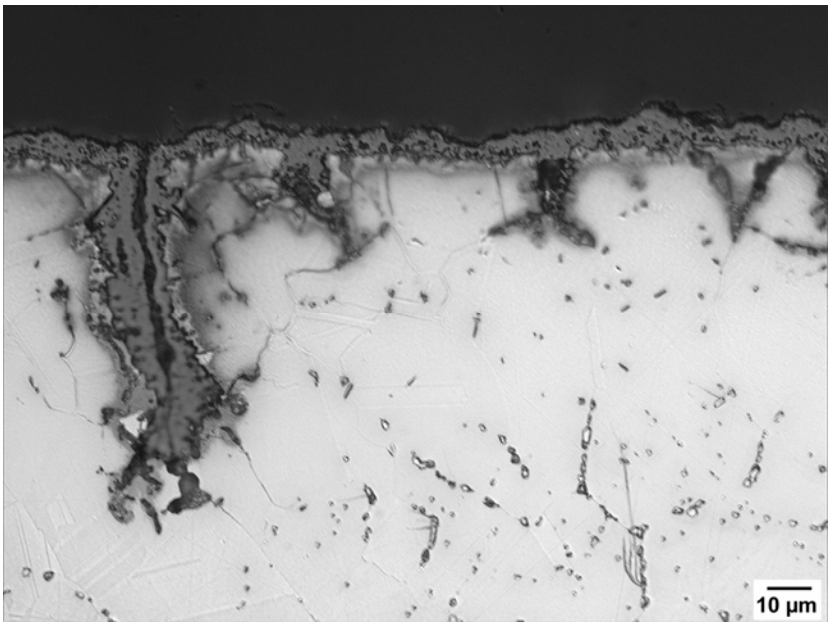

Fig. 39: Surface oxide and secondary cracks in test performed on Alloy 617 base metal in air at 1000°C, 1.0% strain range and 180 s tensile hold.

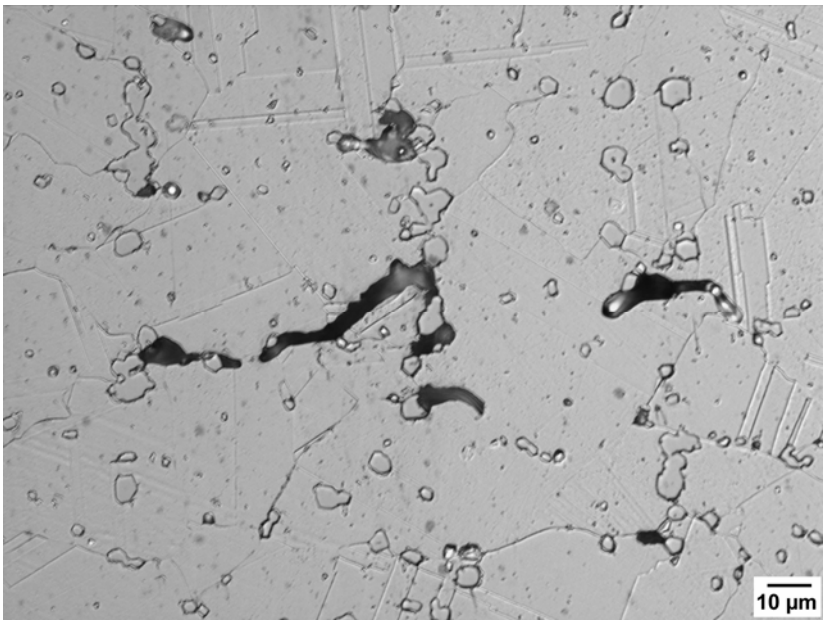

Fig. 40: Grain boundary cavitation initiated at carbides in test performed on Alloy 617 base metal in air 1000°C, 0.3% strain range and 180 s tensile hold.

4.2.2 Base Metal – Vacuum and Inert

Fig. 41 shows creep-fatigue lives for Alloy 617 in vacuum compared against baseline air data. Lives at 1.0% strain range are generally longer in vacuum, while lives in vacuum and air are similar for longer hold times at 0.3%. Vacuum lives are somewhat longer in continuous cycling at 0.3%. Although not shown in the Fig. 41, lives in purified Ar environments at 0.3% strain range and 60 s tensile hold time were essentially the same as in air and vacuum (Table 12).

Significant surface decarburization was observed for all tests performed in inert environments, and oxidation also occurred for tests performed in the purified Ar environments. Oxidation was not observed on specimens tested in vacuum. The degree of decarburization and oxidation varied with the purity of the test environment. After testing at 0.3% strain range with 60 s tensile hold (~100 hr test duration), the depth of decarburization in the specimen tested in vacuum was 175 to 300 µm (the extent varied along the gage length—less decarburization was observed in the vicinity of carbide stringers). For the same test condition the specimen tested in recirculating Ar with the VICI getter had a 10 to 13 µm thick external oxide scale and a 40 to 60 µm decarburized layer; the specimen tested with the SAES getter had a 8 to 10 µm thick external oxide scale and a 400 to 600 µm decarburized layer. Due to the higher circulation rate the purity of Ar using the SAES getter is believed to be higher than that using the VICI getter.

The relative degrees of oxidation and decarburization can be rationalized in terms of the oxidizing potential and its effects on surface scale formation, as described in Ref. [20]. For the lowest purity Ar environment (VICI getter) the oxygen activity is sufficiently high that a

somewhat protective oxide scale is formed, similar to air, and decarburization in minimal. Decarburization results from oxidation of carbides. In the higher purity Ar environment (GC50 getter) the oxide scale formed is not protective and significant decarburization occurs. In vacuum the oxygen potential is even lower and no oxide is formed, but decarburization is less because the total impurity content in the high vacuum is low.

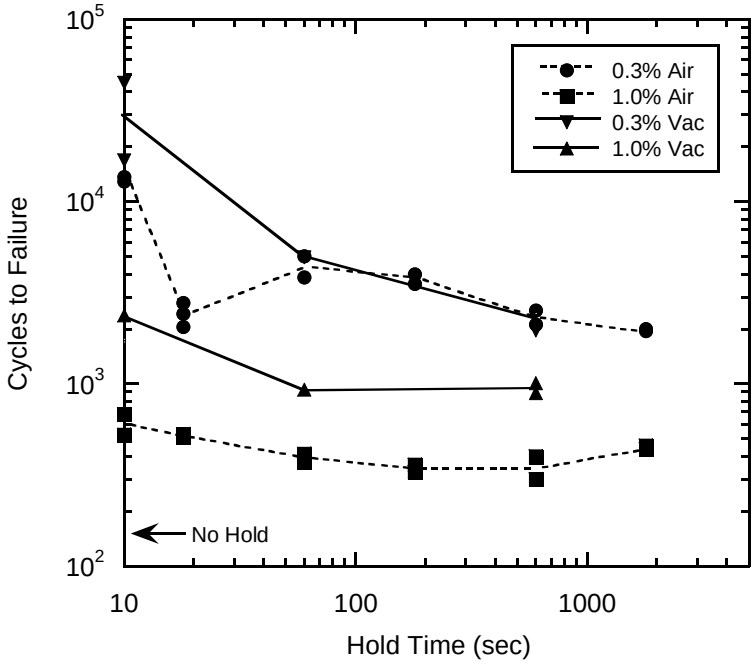

Fig. 41: Cycles to failure versus tensile hold time for Alloy 617 base metal at 1000°C in $3x10^{-5}$ Torr vacuum; air data shown for comparison.

Similar to the behavior in air, cracking in inert environments was intergranular and cavities were observed in tests with tensile hold periods. Figs. 42 and 43 show typical surface layers and secondary cracks observed in two purified Ar environments. The oxides formed in purified Ar were similar in morphology to those formed in air; elemental analysis of the scales has not yet been performed.

4.2.3 Fusion Weldments

Creep-fatigue lives of cross-weld specimens at 800 and 1000°C (1472 and 1832ºF) were consistently lower than for base metal, as shown in Figs. 44 and 45. Reductions in life ranged from factors of approximately 2 to 10, depending on the test condition. Greater reductions were generally observed at longer hold time conditions for both strain ranges and temperatures. Cracks leading to failure in fusion weldment specimens consistently initiated in the weld fusion zones and propagated along interdendritic regions or grain boundaries. Fig. 46 is a low-magnification view of a secondary crack in a specimen tested at 1000°C (1832ºF), 1.0% strain

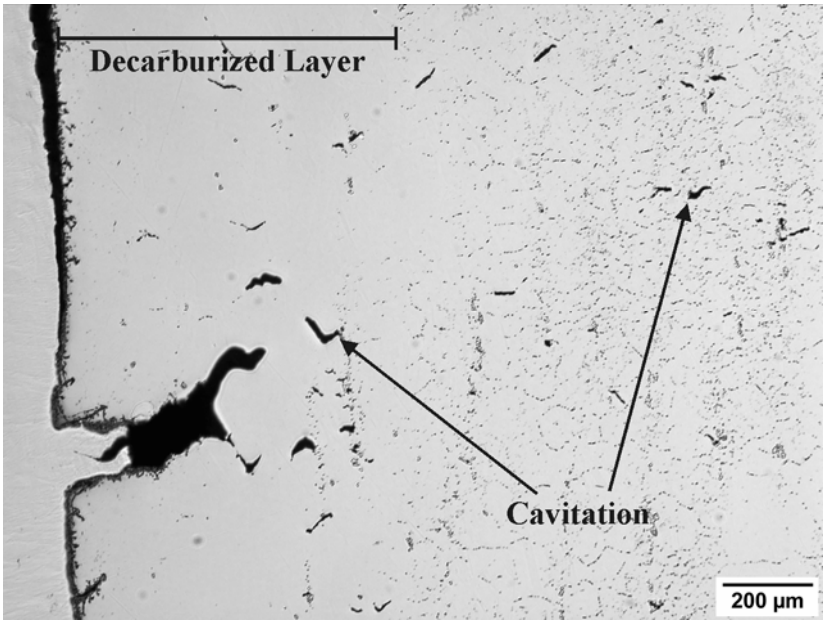

Fig. 42: Decarburized layer, secondary crack, and cavitation formed in purified Ar (GC50 getter) test of alloy 617 base metal at 1000°C, 0.3% strain range and 60 s tensile hold

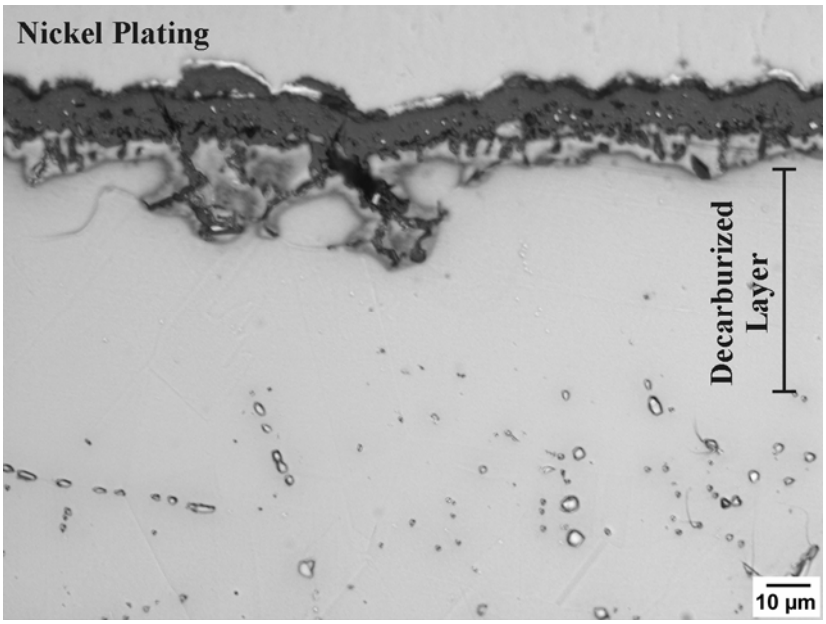

Fig. 43: Oxidation and decarburization layers formed in purified Ar (VICI getter) test of alloy 617 base metal at 1000°C, 0.3% strain range and 60 s tensile hold

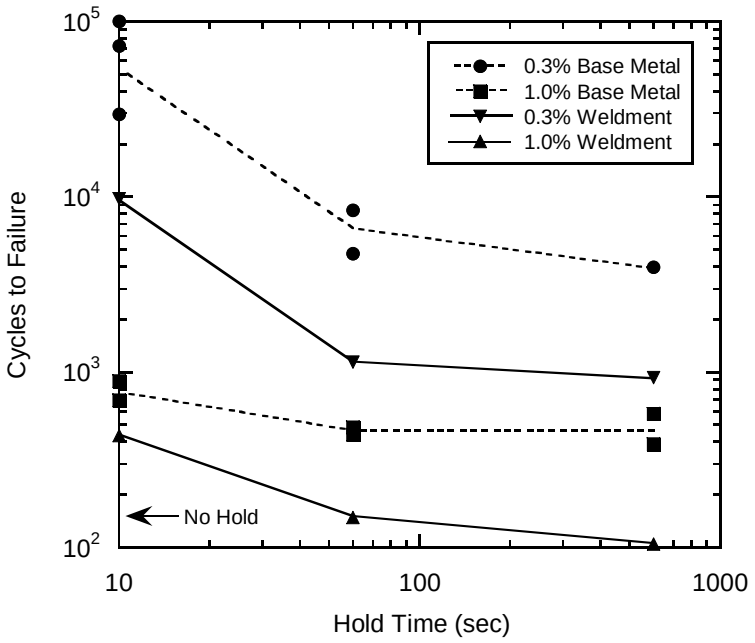

Fig. 44: Cycles to failure versus tensile hold time for alloy 617 fusion weldment at 800°C in air; base metal data shown for comparison

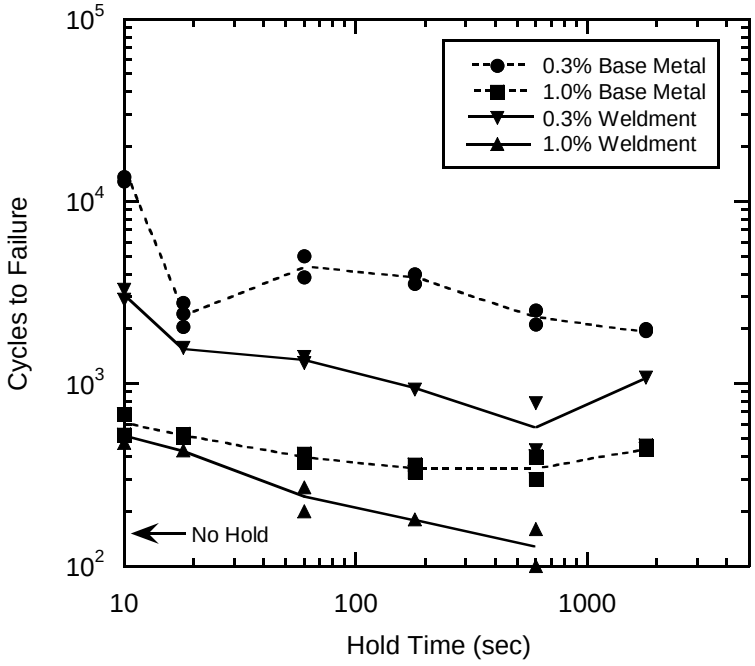

Fig. 45: Cycles to failure versus tensile hold time for alloy 617 fusion weldment at 1000°C in air; base metal data shown for comparison

range, and 600 s hold time illustrating typical crack morphology; Fig. 47 is a higher-magnification view of the crack tip. More detailed analysis of fusion weldment behavior is on-going.

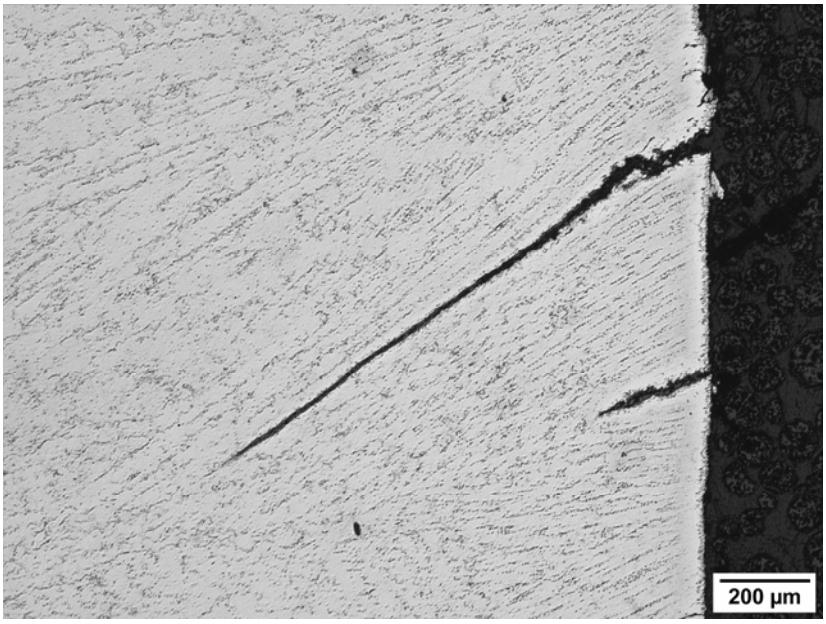

Fig. 46: Secondary cracks in weld fusion zone of Alloy 617 weldment specimen tested in air at 1000°C, 1.0% strain range, 600 s tensile hold

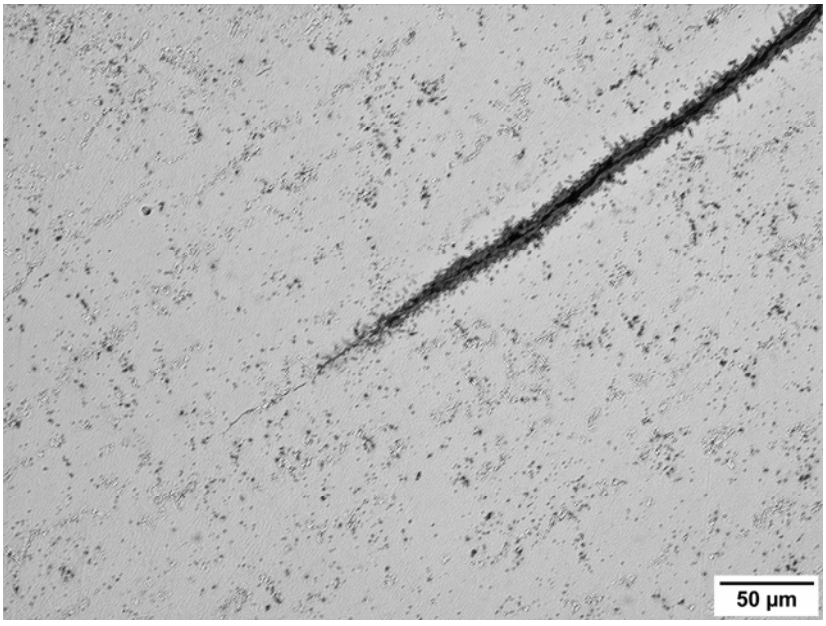

Fig. 47: Close view of tip of large crack shown in Fig. 46

4.3 Future Work

The near-term plans for creep-fatigue testing are to complete repeat tests for fusion weldment specimens in air at 800 and 1000°C (1472 and 1832ºF) and to perform initial tests on Alloy 617 base metal in an impure He environment at 1000°C (1832ºF). For the latter tests a cylinder of impure He has been procured meeting the specification identified in Ref. [21] with the exception of water vapor content. The vendor (Scott Specialty Gases) would not provide certified water vapor content at the level requested (2 ppm). The environmental chamber has been plumbed for testing in flowing impure He gas, and two dewpoint hygrometers have been procured and installed to monitor the moisture content of the gas entering and leaving the chamber.

Creep-fatigue specimens are currently being machined from Alloy 230 base metal and welded plate and CCA 617 plate; baseline testing of these materials in air will be performed starting in FY07. Welded Alloy 230 and Alloy 617 plates from which all-weld-metal specimens can be machined have also been created; creep-fatigue tests will be performed in air to complement the cross-weld tests already performed.

5. BASELINE CHARACTERIZATION OF ALLOY 230 PLATE AT INL (T. Totemeier & D. Clark)

An earlier report [9] described the procurement and manufacturer's certified properties of a 19 mm (0.748") thick plate of Alloy 230. This section presents INL characterization of baseline microstructure, tensile properties, and impact properties of this plate.

5.1 Chemistry and Microstructure

The dimensions of the procured plate were 1.14 × 2.54 m^2 (44.9" x 100") and 19 mm (0.748") thickness; the manufacturer-certified chemical composition is given in Table 15. A three-dimensional montage of the etched optical microstructure is shown in Fig. 48. Stringers of carbides are aligned in the rolling direction. Contrary to the Alloy 617 plate, there is little banding of grain size; the grains are essentially equiaxed, approximately 40 to 120 µm in diameter. The carbides are round and elongated and range in size from approximately 1 to 30 µm. Fig. 49 shows a typical microstructure as seen in backscattered mode in the SEM; a higher-magnification view of a clump of carbide particles is shown in Fig. 50. Semi-quantitative energy-dispersive x-ray spectroscopy (EDS) shows the bright particles in Fig. 50 to be W- and Mo-rich, while the darker gray particles are Cr-rich.

Table 15: Chemical composition of alloy 230 plate and filler weld wire.

Heat	Composition (wt.%)												
	Ni	Cr	W	Mo	Fe	Co	Cu	Al	C	Mn	Si	S	B
8305 5 7896 (19 mm plate)	Bal.	22.43	13.91	1.34	1.34	0.21	0.04	0.29	0.11	0.53	0.37	<0.002	0.004
5706601 (weld wire)	Bal.	21.99	13.81	1.37	1.15	0.06	0.04	0.36	0.07	0.49	0.43	<0.002	--

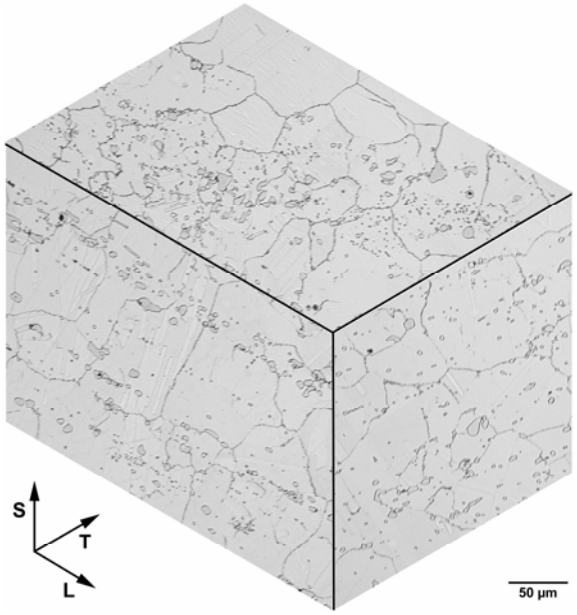

Fig. 48: three-dimensional montage of optical microstructure in Alloy 230

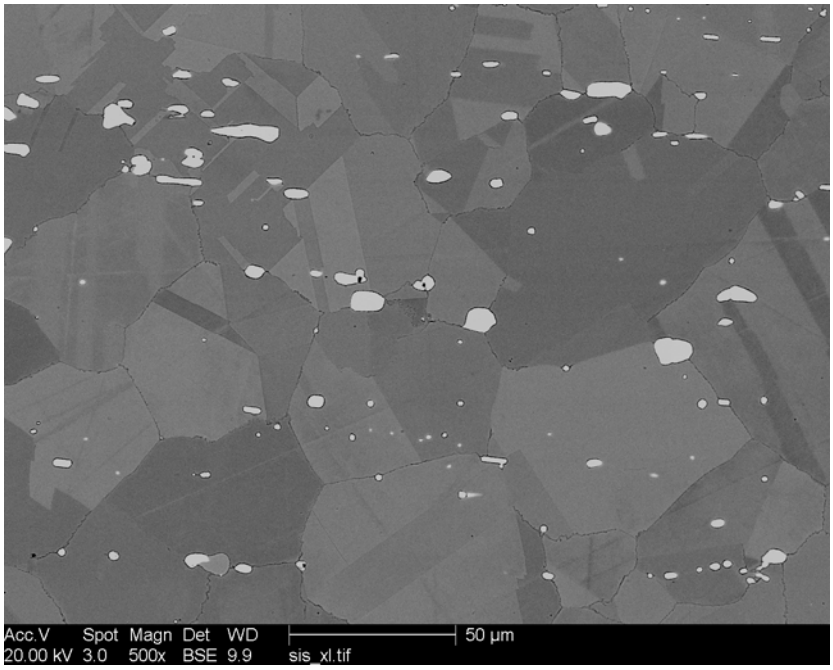

Fig. 49: Typical alloy 230 microstructure; bright particles are W- and Mo-rich carbides, medium grey particle (lower left corner) is Cr-rich carbide. Backscattered electron image

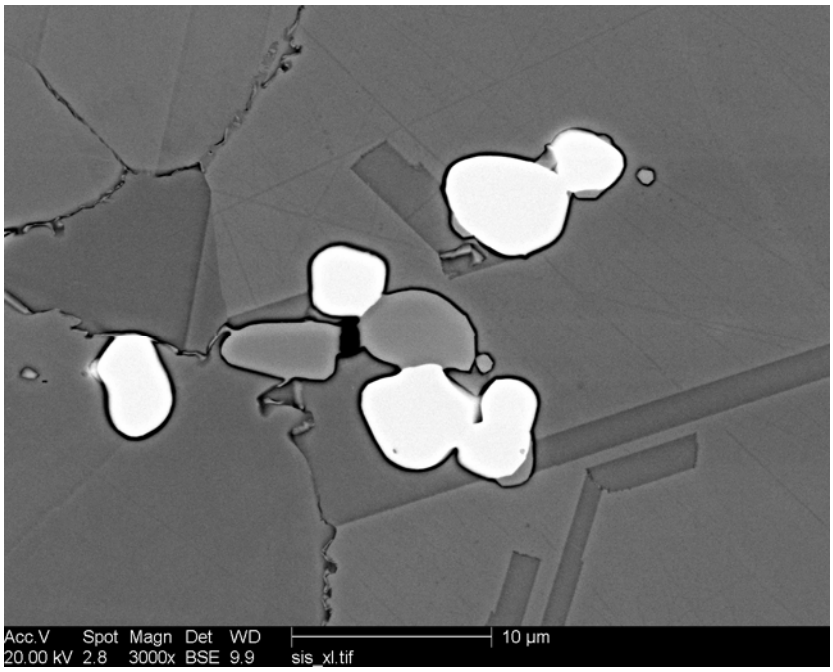

Fig. 50: Close view of carbide cluster, both W- and Cr-rich carbides.

5.2 Tensile and Impact Properties

The results of tensile tests at temperatures of 25, 750, 850, and 950°C (77, 1382, 1562, and 1742ºF) are presented in Table 16. These tests were performed to confirm the manufacturer's certified properties and develop a baseline of properties for this plate at the temperatures of interest. Tests were performed according to the ASTM E 8M standard at a constant cross-head speed corresponding to an initial nominal strain rate of 1×10^{-3} sec^{-1}. Specimens were heated in a radiative furnace with temperature monitored by a Type K thermocouple wired to the gage section. Extension was monitored by a single clip gage at room temperature; an averaging rod-in-tube extensometer was used in elevated temperature tests.

The measured mean room-temperature strength and ductility in both orientations slightly exceeded the certified values for the plate (certified yield strength = 360 MPa, ultimate tensile strength = 820 MPa, ductility = 46%, reduction in area = 43%). Strength was considerably reduced at elevated temperatures, as expected. Tensile ductility did not increase with temperature, although reduction in area did. Serrated flow indicative of dynamic strain aging was observed in tests at 750 and 850°C (1382, 1562ºF). The data sheet for Alloy 230 provided by Haynes indicates continuously-increasing tensile ductility with temperature for hot-rolled and solution-annealed plate, contrary to the current data. Ultimate tensile strengths in the current plate are also lower than given in the data sheet.

Charpy V-notch impact tests were performed according to the ASTM E 23 at room temperature on specimens machined in four different plate orientations: L-T, L-S, T-L, and T-S. The impact test results are listed in Table 17, data for the 20 mm (0.787") thick Alloy 617 plate are shown for comparison. Unlike the Alloy 617 plate, which showed marked anisotropy, the impact strength of the Alloy 230 plate was similar in all orientations, although orientations were the crack propagated across the carbide stringers (e. g., L-S) had slightly higher strength than orientations in which the crack propagated along the carbide stringers (e. g., T-L). All impact strengths for the Alloy 230 plate were lower than the lowest Alloy 617 impact strength (99 J for T-L orientation). The lower impact strength is consistent with the reduced room temperature ductility and reduction in area for Alloy 230 compared with Alloy 617 (~ 60% ductility and 50% reduction in area for Alloy 617).

Table 16: Alloy 230 plate tensile test results

Test/Specimen ID	Orientation	Test Temperature	Elastic Modulus	Yield Stress	UTS	Ductility	RA
		(°C)	(GPa)	(MPa)	(MPa)	(%)	(%)
230-TEN-1	Longitudinal	25	195	396	840	50	46
230-TEN-2	Longitudinal	25	180	410	854	47	45
230-TEN-3	Longitudinal	25	230	415	845	48	46
230-TEN-13	Transverse	25	165	380	841	46	42
230-TEN-14	Transverse	25	215	382	830	45	40
230-TEN-15	Transverse	25	193	424	849	45	41
230-TEN-4	Longitudinal	750	141	270	564	48	57
230-TEN-5	Longitudinal	750	143	278	547	44	59
230-TEN-6	Longitudinal	750	129	283	565	47	58
230-TEN-16	Transverse	750	122	267	531	44	57
230-TEN-17	Transverse	750	126	285	518	45	56
230-TEN-18	Transverse	750	170	275	530	43	57
230-TEN-7	Longitudinal	850	124	253	375	37	68
230-TEN-8	Longitudinal	850	139	268	388	37	68
230-TEN-9	Longitudinal	850	139	260	391	38	69
230-TEN-19	Transverse	850	148	253	369	39	68
230-TEN-20	Transverse	850	133	256	345	43	72
230-TEN-21	Transverse	850	148	265	354	40	71
230-TEN-10	Longitudinal	950	122	228	229	39	71
230-TEN-11	Longitudinal	950	98	226	226	36	71
230-TEN-12	Longitudinal	950	97	234	234	38	73
230-TEN-22	Transverse	950	113	210	210	42	73
230-TEN-23	Transverse	950	111	202	209	40	70
230-TEN-24	Transverse	950	107	212	212	42	73

Table 17: Alloy 230 and Alloy 617 plate impact test results

Specimen Orientation	Charpy Impact Energy (J)	
	Alloy 230	Alloy 617
L-S	92	170
L-T	83	107
T-L	66	99
T-S	81	> 260*

6. JOINING OF ALLOYS 230 AND 617 AT INL (T. Totemeier & D. Clark)

Joining work this fiscal year has included the creation of welded plates of Alloy 230 for cross-weld creep-fatigue test specimens, wide-gap welded plates for all-weld-metal creep-fatigue specimens of Alloy 230 and Alloy 617, and limited investigation of techniques and parameters for high-temperature brazing and diffusion bonding of Alloys 230 and 617.

6.1 Fusion Welding

Three Alloy 230 plates 25 × 38 cm^2 with butt welds down the center of the plate were created using Alloy 230W filler wire (0.11 mm diameter) and the gas-tungsten arc process. The weld joint and welding parameters were identical to those used for the Alloy 617 plate reported in Ref. [17]; the joint design is shown in Fig. 51 and Table 15 lists the certified chemical composition of the weld filler wire. Fig. 52 shows a completed welded plate; a polished metallographic cross-section of the weld joint is shown in Fig. 53. The welded plates were radiographed for defects; none were found. Metallographic characterization of the weld and heat affected zone is in progress.

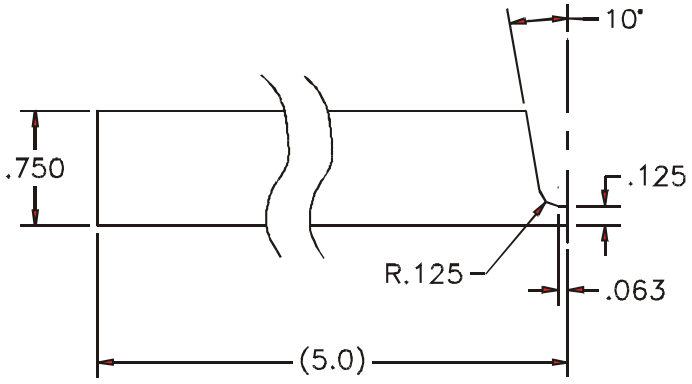

Fig. 51: Fusion weld joint profile. Dimensions in inches

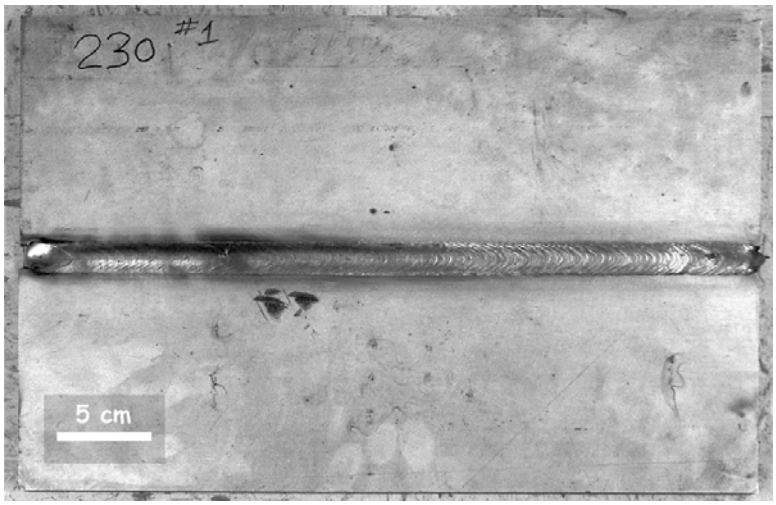

Fig. 52: Welded alloy 230 plate

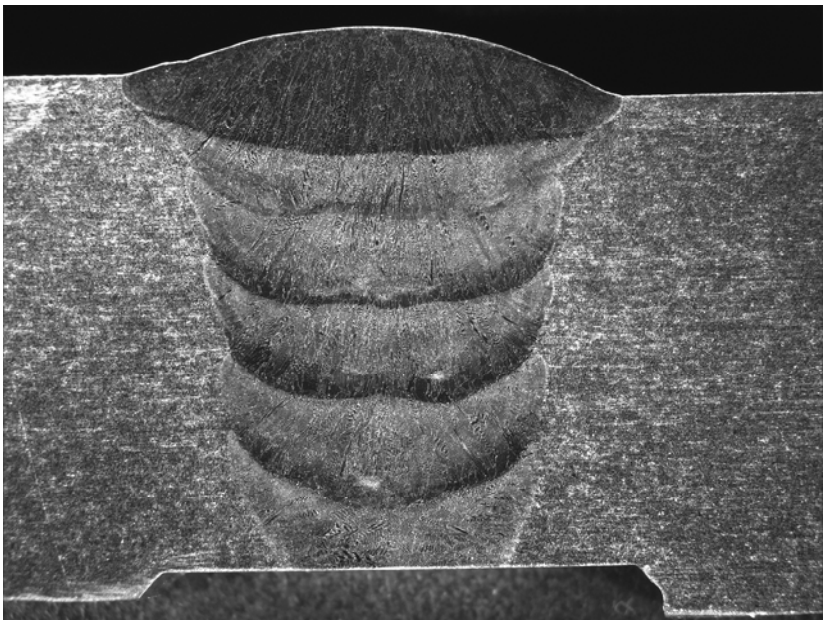

Fig. 53: Etched cross-section of alloy 230 weld. Plate thickness is 19 mm

Alloy 230 and Alloy 617 plates with wide joint gaps were welded using the GTA process. Fig. 54 shows a schematic of the joint, which is sized to allow creep-fatigue test specimens to be machined transverse to the weld for which the reduced section will be entirely weld metal. Significant distortion of the plates occurred during welding; the plates were stress-relieved at 750°C for 2 hours then straightened at room temperature. Fig. 55 shows the Alloy 230 welded wide-gap plate after straightening.

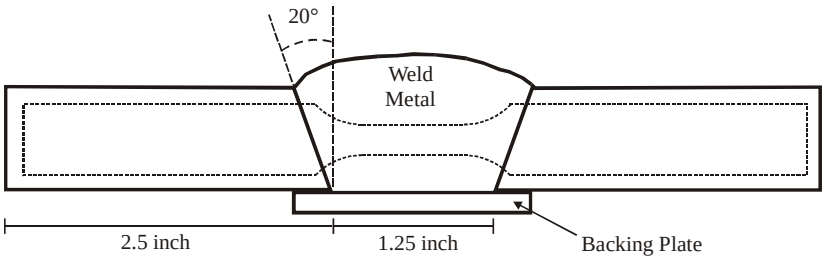

Fig. 54: Schematic of wide-gap weld joint for transverse weld metal creep-fatigue specimens

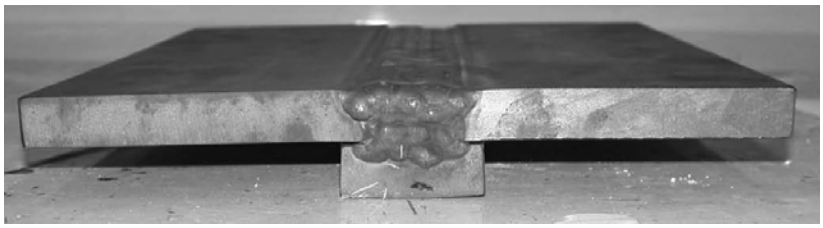

Fig. 55: Wide-gap weld in alloy 230 plate after stress relief and straightening. Plate thickness is 19 mm.

6.2 High-Temperature Brazing

Several attempts to make quality braze joints in Alloys 230 and 617 were made using small pieces and a vacuum furnace. The braze used was AWS BNi-1, a Ni-Cr-Si-B alloy recommended for high-temperature service. Brazing was performed in flowing hydrogen gas at 1100 and 1150°C; a silver brazing flux was used to improve wetting. Good wetting was achieved in all trials, but void formation along the joint has occurred in all trials performed to date, as shown in Fig. 56. In addition, significant grain boundary dissolution was observed in Alloy 617 joints, as shown in Fig. 57. The dissolution is presumed to result from the presence of the flux, since it was not observed in previous trials with Alloy 617 [17]. Current efforts are focusing on joints without flux and with nickel plating if necessary.

6.3 Diffusion Bonding

Two diffusion bonds were created in Alloy 230 using a Gleeble thermo-mechanical simulator to apply heat and force, as described in Ref. [17]. One joint was created without a nickel interlayer at 1150°C with a 2.5 hr hold time and 7 MPa initial stress; a second joint was created with a 15 μm pure nickel interlayer at 1150°C with a 3 hr hold time and 7 MPa initial stress. Good bonding was observed in both joints. Limited grain growth across the joint occurred in the joint without the interlayer, as shown in Fig. 58. More complete grain growth across the joint occurred with the interlayer (Fig. 59). In Alloy 617 no grain growth was observed across the joint without an interlayer; the difference in behavior likely results from the lower Al and Ti content of Alloy 230 compared to Alloy 617.

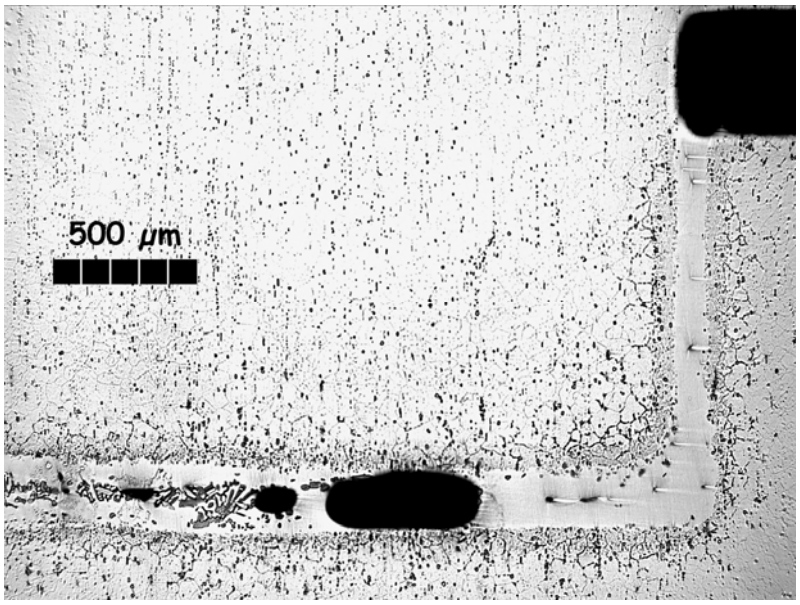

Fig. 56: Polished and etched cross-section of braze joint in alloy 230 illustrating good wetting but porosity in bond

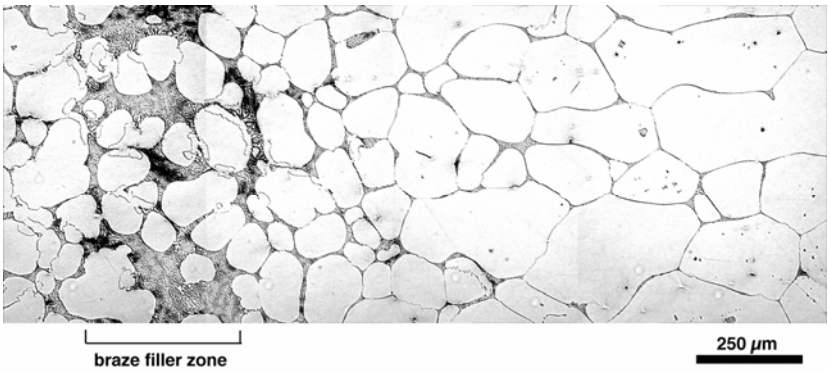

Fig. 57: Cross-section of braze joint in alloy 617 showing grain boundary dissolution

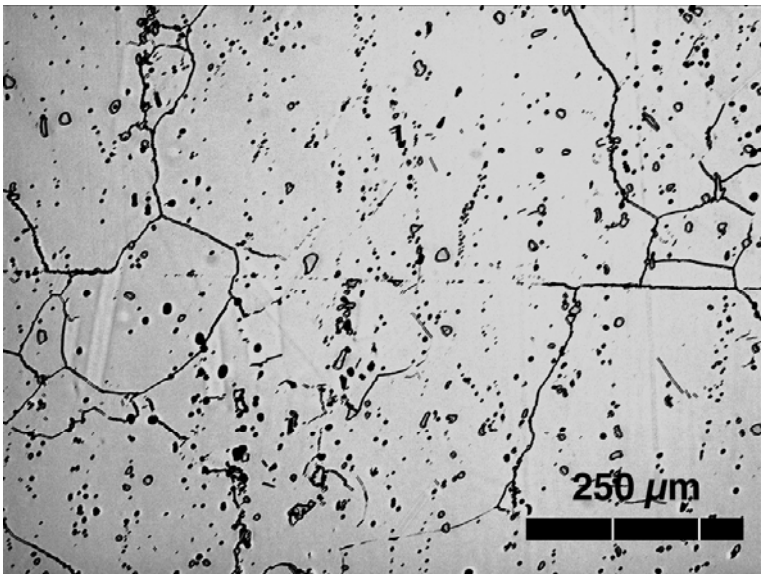

Fig. 57: Cross-section of diffusion bond in alloy 230, no interlayer, 1150° C, 2.5 h, 7 MPa. The bondline is horizontal across the center of the image.

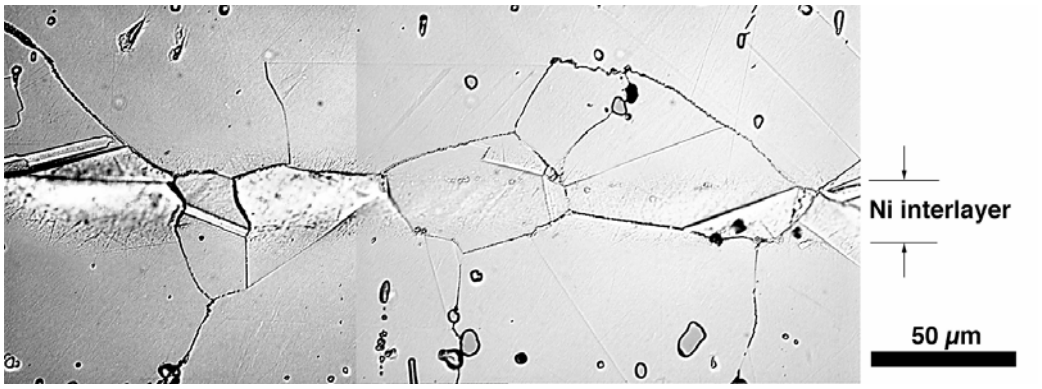

Fig. 59: Cross-section of diffusion bond in alloy 230 with 15 μm nickel interlayer, 1150°C, 3 h, 7 MPa

7. CHARACTERIZATION OF CCA 617

A plate of CCA 617 300 × 300 × 50 mm^3 in dimension was received from ORNL. The plate was sectioned and sent for machining into creep-fatigue specimens. Baseline low-cycle fatigue and creep-fatigue tests are planned to be performed at 850 and 950°C in air.

8. REFERENCES

[1] "Very High Temperature Reactor (VHTR) Survey of Materials Research and Development Needs to Support Early Deployment", INEEL/EXT-03-00141, U. S. Department of Energy Generation IV Nuclear Reactor Program, U. S. Department of Energy, January 31, 2003, Guido Baccaglini et al.

[2] "Updated Generation IV Reactors Integrated Materials Technology Program Plan Revision 2", ORNL/TM-2005/556, U. S. Department of Energy Generation IV Nuclear Reactor Program, U. S. Department of Energy, December 31, 2005, Bill Corwin et al.

[3] "Assessment of Existing Alloy 617 Data for Gen IV Materials Handbook", ORNL/TM-2005/510, U. S. Department of Energy Generation IV Nuclear Reactor Program, U. S. Department of Energy, June 30, 2005, Weiju Ren and Robert W. Swindeman.

[4] "Development of A Controlled Material Specification for Alloy 617 for Nuclear Applications", ORNL/TM-2005/504, U. S. Department of Energy Generation IV Nuclear Reactor Program, U. S. Department of Energy, May 30, 2005, Weiju Ren and Robert W. Swindeman.

[5] "Pressure Vessel Code Construction Capabilities for a Nickel-Chromium-Tungsten-Molybdenum Alloy," pp. 179-187 in New Alloys for Pressure Vessels and Piping, PVP-201, American Society of Mechanical Engineers, New York, NY, 1990, M. F. Rothman.

[6] "The LCF Behavior of Several Solid Solution Strengthened Alloys Used in Gas Turbine Engines," paper ASME 90-GT-80, presented at the Gas Turbine and Aeroengine Congress and Exposition, Brussels, Belgium, June 11-14, 1990, S. K. Srivastava and D. L. Klarstrom.

[7] "The Thermal Fatigue Behavior of the Combustor Alloys IN 617 and HAYNES 230 Before and After Welding," Metall. Trans. 30A, 1999, 981-989, F. Meyer-Olbersleben, N. Kasik, B. Ilschner, and F. Rezai-Aria.

[8] "High Temperature Metallic Materials Test Plan for Generation IV Nuclear Reactors", ORNL/TM-2005/507, U. S. Department of Energy Generation IV Nuclear Reactor Program, U. S. Department of Energy, November 30, 2004, Weiju Ren and Robert W. Swindeman.

[9] "Procurement and Initial Characterization of Alloy 230 and CMS Alloy 617", INL/EXT-06-11290, U. S. Department of Energy Generation IV Nuclear Reactor Program, U. S. Department of Energy, April 2006, Terry Totemeier and Weiju Ren.

[10] "Re: Manufacturing Viability of 617", W. Ren's business email communication with Special Metals, November 4, 2005, Jim Crum.

[11] "A Review of Aging Effects in Alloy 617 for Gen IV Nuclear Reactor Applications", Proceedings of 2006 ASME Pressure Vessels and Piping Division Conference, July 23-27, 2006, Vancouver, British Columbia, Canada, Weiju Ren and Robert Swindeman.

[12] "Rules for Design of Alloy 617 Nuclear Components to Very High Temperatures," pp. 147-153, PVP – Vol. 215, Fatigue, Fracture, and Risk, Am. Soc. of Mechanical Engineers, 1991, J. M. Corum and J. J. Blass.

[13] "Gen IV Materials Handbook Architecture and System Design", ORNL-GEN4/LTR-06-004, U. S. Department of Energy Generation IV Nuclear Reactor Program, U. S. Department of Energy, February 28, 2006, Weiju Ren.

[14] "Initial Development of the Gen IV Materials Handbook", ORNL-GEN4/LTR-05/012, U. S. Department of Energy Generation IV Nuclear Reactor Program, U. S. Department of Energy, September 15, 2005, Weiju Ren and P. Rittenhouse.

[15] "Construction of Web-Accessible Materials Handbook for Generation IV Nuclear Reactors", PVP2005-71780, Proceedings of the 2005 ASME Pressure Vessels and Piping Conference, July 17 – 21, 2005, Denver, Colorado USA, Weiju Ren and Philip Rittenhouse.

[16] "Gen IV Materials Handbook Implementation Plan", ORNL/TM-2005/77, U. S. Department of Energy Generation IV Nuclear Reactor Program, U. S. Department of Energy, March 29, 2005, P. Rittenhouse and Weiju Ren.

[17] "Microstructure and Strength Characteristics of Alloy 617 Welds", INL/EXT-05-00488, 2005, T. C. Totemeier, H. Tian, D.E. Clark, and J. A. Simpson.

[18] "Status of Creep-Fatigue Testing of Welded Alloy 617 Specimens in Support of the NGNP", INL/EXT-05-00781, 2005, T. C. Totemeier.

[19] "Procurement and Checkout of Environmental Chamber for Creep-Fatigue Test Frame in Support of the NGNP", INL/EXT-05-00782, 2005, T. C. Totemeier.

[20] "Werkstoffe und Korrosion", 1985, vol. 36, pp. 141-50, W. J. Quadakkers and H. Schuster.

[21] "Aging and Environmental Test Plan", ORNL/TM-2005/523, 2005, Dane F. Wilson, Weiju Ren, Tim E. McGreevy, Richard N. Wright, and Terry C. Totemeier.

APPENDIX

Letter to Alstom Power for CCA Alloy 617 Acquisition and Data Sharing

OAK RIDGE NATIONAL LABORATORY
MANAGED BY UT-BATTELLE FOR THE DEPARTMENT OF ENERGY

Weiju Ren, Ph. D.
Oak Ridge National Laboratory
MS-6155, Bldg. 4500-S
Oak Ridge, TN 37831
Phone: 865-576-6402
Email: renw@ornl.gov

February 10, 2006

Jeff Henry
Alstom Power
1119 Riverfront Parkway
Chattanooga, TN 37402

Dear Mr. Henry,

Per our discussion at the Portland Code meeting, I understand that Alstom Power has ownership of the CCA 617 alloy and needs a written request from ORNL to consider collaboration in testing and data sharing with the DOE Gen IV Nuclear Reactor Materials Program.

To my knowledge, the material has been tested at temperatures up to 800°C at ORNL for the DOE Ultra Supercritical Boiler Materials Program for building fossil power plants. The goal of DOE's reactor program is to develop advanced nuclear power plants. Both programs have a common goal to prepare the material for ASME codification, if the material indeed exhibits improved properties for power plant applications. In this regard, both programs share some of the same data needs, with the Gen IV program needing a wider temperature range, up to 1000°C. Based on these facts, we believe that collaboration in testing and data sharing between these two programs would be technically viable and financially efficient. As Altrom Power is a member of a consortium of boiler manufacturers working on the DOE Ultra Supercritical Boiler Materials Program, would you please present the request to them on our behalf if it is necessary to obtain the consortium's approval?

To initiate the collaboration, I would like to propose the following plan:

Alstom Power provides the CCA 617 material at no cost to ORNL to generate data and fill data gaps for improved properties verification and ASME codification. In return, ORNL provides Alstom Power with the data generated as part of the Gen IV Reactor Program at no cost to the Fossil program or other applications. Due to its experimental nature, neither party will hold the other legally liable for the accuracy, completeness or usefulness of the data provided.

In parallel to this cooperation, we will work with the Ultrasupercritical Boiler Materials Consortium to more fully share the data generated to date.

The material ORNL needs at present is a 2" x 12" x 5' plate of CCA 617. I greatly appreciate your kind considerations of the collaboration. If you have any questions or would like to discuss further details, please feel free to contact me.

Sincerely,

Weiju Ren
Cc: Bill Corwin, George Hayner, Roddie Judkins, John Shingledecker

DISTRIBUTION

1. T. D. Burchell
2. R. Battiste
3. W. R. Corwin
4. S. R. Greene
5. D. T. Ingersoll
6. Y. Katoh
7. J. W. Klett
8. E. Lara-Curzio
9. L. K. Mansur
10. T. E. McGreevy
11. R. K. Nanstad
12. R. A. Raschke
13. W. Ren
14. P. L. Rittenhouse
15. A. F. Rowcliff
16. M. Santella
17. L. L. Snead
18. R. G. Stoller
19. R. W. Swindeman
20. P. F. Tortorelli
21. D. F. Wilson
22. S. J. Zinkle

23. Cathy Barnard, Idaho National Laboratory, P.O. Box 1625, Idaho Falls, Idaho 83415-3750

24. Trevor Cook, NE-20/Germantown Building, Office of Advanced Nuclear Research, U.S. Department of Energy, 1000 Independence Avenue, S.W., Washington, DC 20585-1290

25. Dennis Clark, Idaho National Laboratory, P.O. Box 1625, Idaho Falls, ID 83415-2210

26. Susan Lesica, NE-20/Germantown Building, Office of Advanced Nuclear Research, U.S. Department of Energy, 1000 Independence Avenue, S.W., Washington, DC 20585-1290

27. Thomas J. O'Conner, NE-20/Germantown Building, Office of Advanced Nuclear Research, U.S. Department of Energy, 1000 Independence Avenue, S.W., Washington, DC 20585-1290

28. Rafael Soto, Idaho National Laboratory, P.O. Box 1625, Idaho Falls, Idaho 83415-3750

29. Terry Totemeier, Idaho National Laboratory, P.O. Box 1625, Idaho Falls, ID 83415-2218

30 Robert Versluis, NE-20/Germantown Building, Office of Advanced Nuclear Research, U.S. Department of Energy, 1000 Independence Avenue, S.W., Washington, DC 20585-1290

31 Kevan Weaver, Idaho National Engineering and Environmental Laboratory, P.O. Box 1625, Idaho Falls, Idaho 83415-3750